PIK3Cδ expression by fibroblasts promotes triple-negative breast cancer progression

Teresa Gagliano,[1] Kalpit Shah,[2] Sofia Gargani,[3] Liyan Lao,[4] Mansour Alsaleem,[5] Jianing Chen,[4] Vasileios Ntafis,[3] Penghan Huang,[4] Angeliki Ditsiou,[1] Viviana Vella,[1] Kritika Yadav,[6] Kamila Bienkowska,[1] Giulia Bresciani,[1,7] Kai Kang,[8] Leping Li,[8] Philip Carter,[9] Graeme Benstead-Hume,[10] Timothy O'Hanlon,[11] Michael Dean,[2] Frances M.G. Pearl,[10] Soo-Chin Lee,[6,12,13] Emad A. Rakha,[5] Andrew R. Green,[5] Dimitris L. Kontoyiannis,[3,14] Erwei Song,[4] Justin Stebbing,[9] and Georgios Giamas[1]

[1]Department of Biochemistry and Biomedicine, School of Life Sciences, University of Sussex, Falmer, Brighton, United Kingdom. [2]Division of Cancer Epidemiology and Genetics, National Cancer Institute, NIH, Bethesda, Maryland, USA. [3]Division of Immunology, Biomedical Sciences Research Center Alexander Fleming, Vari, Greece. [4]Breast Tumor Center, Sun Yat-Sen Memorial Hospital, Sun Yat-Sen University, Guangzhou, China. [5]Nottingham Breast Cancer Research Centre, Division of Cancer and Stem Cells, School of Medicine, Nottingham City Hospital, University of Nottingham, Nottingham, United Kingdom. [6]Cancer Science Institute of Singapore, National University of Singapore, Singapore. [7]Department of Medical Sciences, University of Ferrara, Ferrara, Italy. [8]Biostatistics and Computational Biology Branch, National Institute of Environmental Health Sciences, NIH, Durham, North Carolina, USA. [9]Division of Cancer, Department of Surgery and Cancer, Imperial College London, Hammersmith Hospital Campus, London, United Kingdom. [10]Bioinformatics Group, School of Life Sciences, University of Sussex, Falmer, Brighton, United Kingdom. [11]Cancer Genomics Research Laboratory, Frederick National Laboratory for Cancer Research, Bethesda, Maryland, USA. [12]Department of Haematology-Oncology, National University Cancer Institute, Singapore. [13]National University Health System, Singapore. [14]Department of Genetics, Development and Molecular Biology, School of Biology, Aristotle University of Thessaloniki, Thessaloniki, Greece.

As there is growing evidence for the tumor microenvironment's role in tumorigenesis, we investigated the role of fibroblast-expressed kinases in triple-negative breast cancer (TNBC). Using a high-throughput kinome screen combined with 3D invasion assays, we identified fibroblast-expressed PIK3Cδ (f-PIK3Cδ) as a key regulator of cancer progression. Although PIK3Cδ was expressed in primary fibroblasts derived from TNBC patients, it was barely detectable in breast cancer (BC) cell lines. Genetic and pharmacological gain- and loss-of-function experiments verified the contribution of f-PIK3Cδ in TNBC cell invasion. Integrated secretomics and transcriptomics analyses revealed a paracrine mechanism via which f-PIK3Cδ confers its protumorigenic effects. Inhibition of f-PIK3Cδ promoted the secretion of factors, including PLGF and BDNF, that led to upregulation of NR4A1 in TNBC cells, where it acts as a tumor suppressor. Inhibition of PIK3Cδ in an orthotopic BC mouse model reduced tumor growth only after inoculation with fibroblasts, indicating a role of f-PIK3Cδ in cancer progression. Similar results were observed in the MMTV-PyMT transgenic BC mouse model, along with a decrease in tumor metastasis, emphasizing the potential immune-independent effects of PIK3Cδ inhibition. Finally, analysis of BC patient cohorts and TCGA data sets identified f-PIK3Cδ (protein and mRNA levels) as an independent prognostic factor for overall and disease-free survival, highlighting it as a therapeutic target for TNBC.

Introduction

Triple-negative breast cancer (TNBC; ER^-, PR^-, $HER2^-$) represents a molecularly diverse and highly heterogeneous subtype of breast cancer (BC) (15%–20%) with a poor prognosis and high rates of recurrence and metastasis. Treatment largely relies on chemotherapy, which remains toxic and often ineffective (1, 2).

Despite mounting evidence for the role of the tumor microenvironment (TME) in affecting surrounding cells and its involvement in metastatic progression, little is known about how stromal cells can influence the behavior of cancer epithelial cells and how they affect their response to target therapy (3–5). Under physiological conditions, the stroma serves as a barrier to epithelial cell transformation, while the interplay between epithelial cells and the microenvironment can maintain epithelial polarity and modulate growth inhibition (6). In BC, gene expression analysis of the tumor stroma has led to identification of clusters that can predict clinical outcome (7). In TNBC patients, infiltration of inflammatory cells or the presence of a stroma with reactive, invasive properties has been associated with a poor prognosis (8, 9).

Fibroblasts are the most prominent cells in the TME and can induce both beneficial and adverse effects in premetastatic progression (4, 10). The important functions of fibroblasts include the deposition of extracellular matrix (ECM), regulation of epithelial differentiation, regulation of inflammation, and involvement in cell migration (11, 12). Fibroblast-secreted ECM proteins play a vital role in BC onset and progression (13), while cancer-associated fibroblasts (CAFs) have been shown to promote resistance to cytotoxic and target therapy by secreting protective factors (14). Further understanding the involvement of stromal cells in TNBC, in particular elucidating the crosstalk between fibroblasts and BC cells, might lead to the design

Authorship note: KS and SG contributed equally to this study.
Conflict of interest: JS sits on scientific advisory boards for Celltrion, Singapore Biotech, Vor Biopharma, TLC Biopharmaceuticals, and Benevolent AI; has consulted with Lansdowne Partners, Vitruvian, and Social Impact Capital; and chairs the Board of Directors for BB Biotech Healthcare Trust and Xerion Healthcare.

Submitted: October 28, 2019; **Accepted:** February 27, 2020; **Published:** May 11, 2020.
Reference information: *J Clin Invest*. 2020;130(6):3188–3204.
https://doi.org/10.1172/JCI128313.

of new therapeutic strategies and more effective tailored treatments for TNBC patients.

Finak et al. reported that functional inactivation of PTEN, leading to phosphoinositide 3-kinase (PI3K) activation, in fibroblasts within the breast TME contributes to cancer development and progression (7). We hypothesized that PI3K activity may be a regulator of the tumor-stroma interactions (15) and inhibition of PI3K signaling in fibroblasts could impede its tumor-promoting activity. PI3Ks phosphorylate inositol lipids and are involved in immune response (16–18). Whereas PIK3Cα (p110α) and PIK3Cβ (p110β) are ubiquitously expressed, PIK3Cδ (p100δ) is predominantly expressed in white blood cells (19). However, an unexpected role of PIK3Cδ in oncogenesis of non-hematopoietic cells was observed in avian fibroblasts, where overexpression of wild-type PIK3Cδ induced oncogenic transformation (20, 21). Another report has demonstrated the involvement of PI3K isoforms (including PIK3Cδ) in the differentiation of human lung fibroblasts into myofibroblasts (22). PIK3Cδ contributes to neutrophil accumulation in inflamed tissue by impeding chemoattractant-directed migration as well as adhesive interactions between neutrophils and cytokine-stimulated endothelium (23). Although hampering the activity of PI3Ks in fibroblasts would be expected to inhibit stroma-mediated tumor-promoting activity, a direct effect of PI3K inhibitors on these cells has not been tested to date.

Herein, using a high-throughput siRNA kinome screening, we identify fibroblast-expressed PIK3Cδ as a mediator of TNBC development in vitro and in vivo, and we show the mechanism through which fibroblast PIK3Cδ modulates TNBC progression. Our work reveals a previously uncharacterized yet significant role of fibroblast-expressed PIK3Cδ, which supports the rationale for clinical use of PIK3Cδ inhibitors for the treatment of TNBC.

Results

Cancer-associated markers in HMF and MRC5 fibroblast cell lines. The primary aim of this work was to examine how normal fibroblasts (NFs) within the TME affect TNBC progression. This reflects several controversial issues that have been raised about the genomic landscape of CAFs and the identification of specific markers that differentiate CAFs. According to recent evidence (8), CAFs in TNBC should be characterized by the combined expression of fibroblast-activated protein (FAP), integrin β_1 (ITGβ1/CD29) S100A4, PDGFRβ, α-smooth muscle actin (α-SMA), and caveolin. Therefore, the expression of CAF markers was evaluated in the fibroblast cell lines used herein, HMF and MRC5, and was also compared with that in primary fibroblasts (NFs and CAFs) obtained from 4 TNBC patients (Supplemental Table 1; supplemental material available online with this article; https://doi.org/10.1172/JCI128313DS1). The separation of primary CAFs from NFs was based on the distance from the site of the primary tumor (CAFs < 5 cm; NFs > 5 cm).

As shown in Supplemental Figure 1A, PDGFRβ was more abundant in CAFs compared with NFs, while caveolin was downregulated in CAFs. Overall expression and changes in FAP levels were related to patient variability rather than the fibroblast site of origin. ITGβ1 and α-SMA were widely expressed in all samples, while S100A4 was hardly detectable in primary fibroblasts. The expression levels of the CAF markers in HMF and MRC5 were comparable to those in the primary fibroblast cell lines. PDGFRβ, ITGβ1, FAP, caveolin, and α-SMA were equally detected in HMF and MRC5 cells, while S100A4 was solely present in HMF.

Although the expression levels of these markers in HMF and MRC5 were comparable to those found in primary fibroblasts of TNBC tumors, there was no clear distinction between NFs and CAFs based on these proteins, which supports the aforementioned controversy. In contrast, the similarities between HMF/MRC5 and primary fibroblasts in the expression of CAF markers support the use of these cells as a model to study cancer cell–fibroblast interactions. Nevertheless, since our goal was not restricted to a specific fibroblast subtype, we used both HMF and MRC5 in our experiments.

High-throughput RNAi screening identifies fibroblast-expressed kinases involved in TNBC cell invasion. Based on the established role of protein kinases (PKs) as drug targets and considering the fact that intra- and extracellular signaling is mainly transmitted through PKs, we investigated the role of fibroblast-expressed kinases on TNBC progression. Hence, we established an experimental pipeline (Figure 1A), broadly applicable to different systems, that consisted of a 3D coculturing model (cancer and stromal cells) linked to an invasion assay as a readout tool.

The primary screening was performed in duplicate in HMF and once in MRC5 cells. Fibroblast cell lines were transfected with a pool of 3 siRNAs/gene targeting each of the 710 human kinases (Figure 1A; step 1). Twenty-four hours after transfection, HMF or MRC5 cells were cocultured in 3D with MDA-MB-231, and after 3 days (required for spheroid formation), Matrigel and chemoattractants were added to the wells to promote invasion (Figure 1A, step 2; Supplemental Figure 2, and Supplemental Videos 1 and 2). Pictures of spheroids taken after 3 and 6 days were analyzed, and the results were expressed as changes in spheroid surface (Δ = surface$_{day6}$ – surface$_{day3}$). The Δ value of each silenced kinase (Δ_K) was compared with the Δ value of the control (Δ_{CT}), at different time points, to obtain a Δ_{ratio} ($\Delta_{ratio} = \Delta_{CT}/\Delta_K$) (Figure 1A; step 3). Kinases were divided depending on their effects on MDA-MB-231 invasion, and those with a Δ_{ratio} less than or equal to 0.5 (50% less invasion vs. CT) and *P* less than 0.01 (as well as SD < 0.5 for HMF) were considered as "invasion-promoting," while kinases with a Δ_{ratio} greater than 2 (100% more invasion vs. CT) and *P* greater than 0.05 (as well as SD > 0.5 for HMF) were considered as "invasion-inhibiting" ones. The Δ_{ratio} values were used to calculate the *Z* scores, and all hits were plotted for both cell lines, revealing new potential fibroblast-expressed kinases able to modulate TNBC cell invasion (Figure 1B and Supplemental Figure 3; step 4). All screening data are presented in Supplemental Table 2.

Based on prespecified cutoff criteria, we identified 17 kinases in HMF and 64 in MRC5 cells whose silencing decreased the rate of TNBC invasion (~40%–90%), suggesting a proinvasive role of these proteins (Figure 2A). Under these conditions, there were 2 shared targets among HMF and MRC5: PIK3Cδ and AURKA. Using a panel of fibroblasts and BC cells, we analyzed the levels of PIK3Cδ and AURKA and discovered a variability in their expression among the primary and immortalized fibroblast cell lines (Figure 2B and Supplemental Figure 1B). PIK3Cδ protein levels in fibroblast cells were comparable to those in the BJAB B cell line (used as a positive control) (24), while, intriguingly, PIK3Cδ was hardly detectable or totally absent in most of the BC cells, as

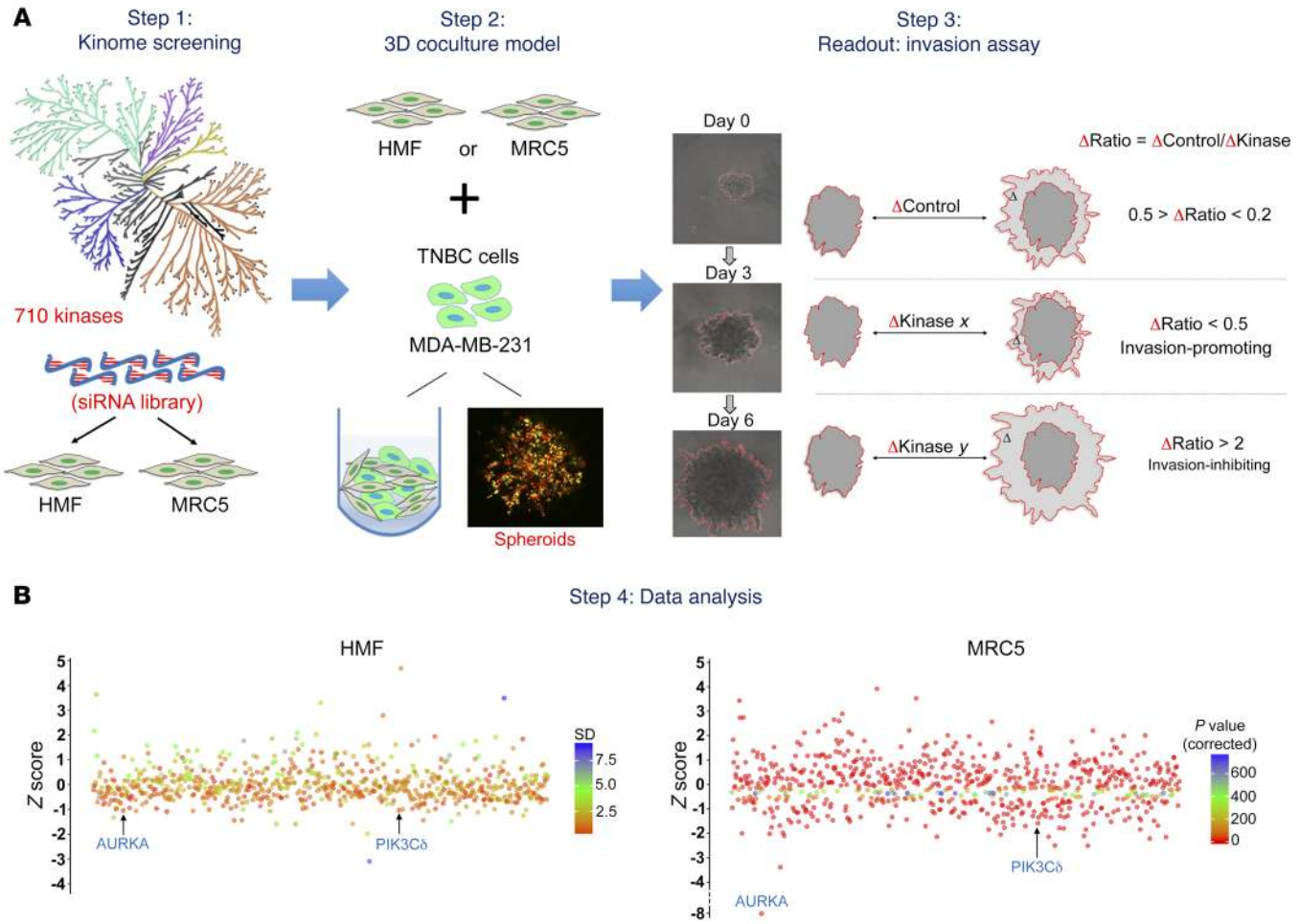

Figure 1. Experimental design of siRNA kinome screening and identification of fibroblast-expressed kinases affecting TNBC invasion. (**A**) Step 1: Silencing of 710 kinases in HMF and MRC5 cells using a siRNA kinome library. Step 2: 3D coculture of HMF or MRC5 with MDA-MB-231 in the presence of Matrigel and chemoattractants to promote invasion. A representative image of cells stained with different fluorescent lipophilic tracers is shown: MDA-MB-231 (red/DiRDiIC18) and MRC5 (green/DiOC6). Step 3: The invasive potential of MDA-MB-231 cells was used as a readout tool. Results are expressed as changes in spheroid surface between day 6 and day 3 ($\Delta_{ratio} = \Delta_{CT}/\Delta_{K}$). The Δ_{ratio} values were used to calculate the *Z* scores based on the formula $Z = (x - \mu)/\sigma$, where μ is Δ_{ratio} mean of 710 kinases, σ is standard deviation (SD), and x is Δ_{ratio} value for each kinase. For HMF, the Δ_{ratio} *Z* score color code refers to SD, as the screening was performed twice, while for MRC5 the Δ_{ratio} *Z* score color code refers to *P* value. (**B**) Step 4: The *Z* scores for HMF and MRC5 are shown. Kinases were divided depending on their effects on MDA-MB-231 invasion. Invasion-promoting: $\Delta_{ratio} \leq 0.5$, $P < 0.01$ (as well as SD < 0.5 for HMF). Invasion-inhibiting: $\Delta_{ratio} > 2$, $P > 0.05$ (as well as SD > 0.5 for HMF).

opposed to AURKA, which was ubiquitously expressed (Figure 2C, Supplemental Figure 1C, and Supplemental Figure 4D, upper panel). Quantitative reverse transcriptase PCR (qRT-PCR) analysis of PIK3Cδ revealed a similar trend for most of the cell lines tested (Supplemental Figure 4A), though it is well known that protein and mRNA abundances do not always correlate (25, 26). Moreover, RNA sequencing (RNA-Seq) in different organs obtained from the Human Protein Atlas (27) revealed that, apart from myeloid and lymphoid cells, fibroblast cell lines express moderate/high PIK3Cδ mRNA levels, in contrast to BC cell lines, which have low/negligible mRNA transcripts (Supplemental Figure 4B). We also investigated whether fibroblast PIK3Cδ can induce the expression of PIK3Cδ in TNBC following extended coculturing between the different cell types. As shown in Supplemental Figure 4, C and D, using both fibroblast cell lines and primary CAFs derived from MMTV-PyMT tumors, there were no changes of PIK3Cδ in TNBC cells, maintaining their low/undetectable protein levels.

Altogether, these results suggest that PIK3Cδ could not have been identified if we had solely studied BC cells instead of examining their interactions with the surrounding stroma, further supporting the setup of our experimental approach regarding cancer as a systemic disease dependent on multiple cell types. We further validated the involvement of fibroblast PIK3Cδ–mediated TNBC 3D invasion by repeating the experiment following silencing (Figure 2D) or overexpression (Figure 2E) of PIK3Cδ. Similar data were obtained using MDA-MB-231, BT-549, and fibroblast cell lines (Supplemental Figure 5, A–F). Finally, we determined that treatment of TNBC cells with conditioned medium (CM) derived from genetically modified fibroblasts (PIK3Cδ-silenced or PIK3Cδ-overexpressed) has no significant effect on TNBC cell proliferation (Supplemental Figure 5G). Taking everything into consideration and bearing in mind the potential implication in BC, we focused on PIK3Cδ and investigated its fibroblast involvement.

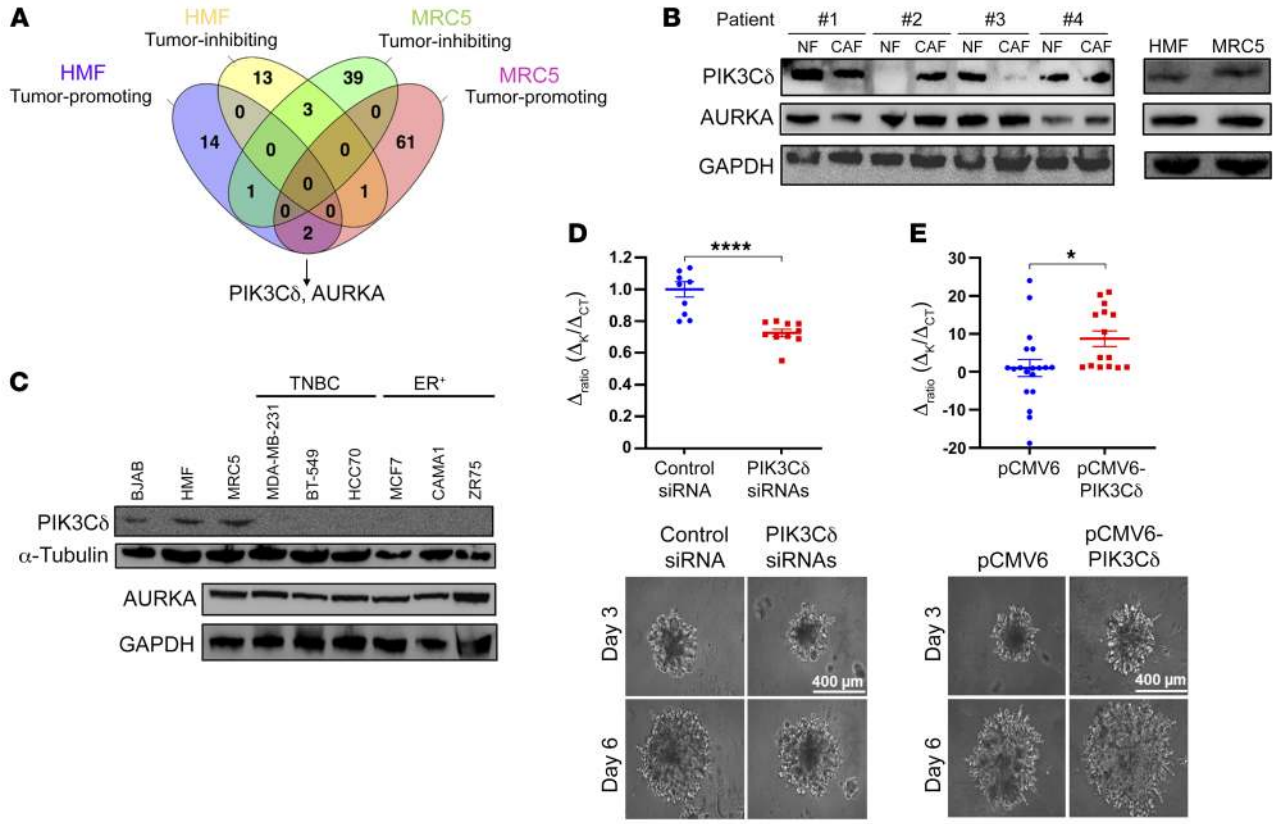

Figure 2. Involvement of fibroblast-expressed PIK3Cδ in TNBC invasion. (**A**) Venn diagram comparing the number of invasion-promoting and invasion-inhibiting kinases in HMF and MRC5 cells. (**B**) Western blotting of PIK3Cδ and AURKA in HMF, MRC5, and primary fibroblasts obtained from TNBC patients. GAPDH was used as loading control. (**C**) Western blotting of PIK3Cδ and AURKA in BC and fibroblast cell lines (BJAB B cell line was used as positive control for PIK3Cδ expression). GAPDH and α-tubulin were used as loading controls. (**D**) Validation of effects of PIK3Cδ knockdown in MRC5 on MDA-MB-231 invasion following the experimental procedure described above (n = 3 independent experiments, minimum 3 technical replicates). Results are expressed as mean ± SEM. Significance was calculated using unpaired t test; ****$P < 0.0001$ vs. control siRNA. (**E**) Effects of PIK3Cδ overexpression in MRC5 cells, using the pCMV6-AC-PIK3Cδ-GFP plasmid, on MDA-MB-231 invasion following the experimental procedure described above (n = 3 independent experiments, minimum 3 technical replicates). Results are expressed as mean ± SEM. Significance was calculated using unpaired t test; *$P < 0.05$ for control siRNA vs. pCMV6-transfected fibroblasts.

Confirmation of high-throughput RNAi screening results. The accuracy and validity of our experimental pipeline/screening was supported by identification of kinases (positive hits) whose involvement in stroma-mediated cancer invasion has been previously reported. Among these results were FLT4 (28) and EGFR (29) (invasion-promoting) as well as ACVR1B (30) and ITPKB (31) (invasion-inhibiting).

To further validate the high-throughput RNAi screening results, we performed the experimental pipeline by using shRNA plasmids targeting randomly selected kinases. As shown in Supplemental Figure 6A, the effects of shRNA-mediated silencing of the tested kinases on the invasion of MDA-MB-231 cells in MRC5 cells were similar to the effects observed in the primary screening. The gene knockdown efficiency was confirmed by real-time qRT-PCR (Supplemental Figure 6B).

Next, we examined the effects of 8 specific inhibitors against the randomly selected and shRNA-validated kinases that affected invasion in the MRC5 screening and repeated the experiment. As anticipated, similar results were observed, although in some cases (e.g., AZD4547) the results were not identical to those of the primary screening (Supplemental Figure 6C). This could be (a) due to potential off-target effects of some inhibitors, (b) due to the fact that some inhibitors can target other isoforms of a specific kinase, and/or (c) because the genomic versus the chemical/pharmacological inhibition of a kinase does not necessarily have the same outcome.

Regarding the overlapping hits from our screening (PIK3Cδ and AURKA), we verified that the observed effects on MDA-MB-231 cell invasion, following genomic inhibition (siRNA), were not based on a reduction (Supplemental Figure 6D) or an increase (PIK3Cδ overexpression; Supplemental Figure 6E) of cell viability.

Genomic or chemical inhibition of PIK3Cδ in fibroblasts reduces TNBC cell invasion as a result of paracrine signaling. To clarify whether the catalytic activity of PIK3Cδ is required for its effect on TNBC progression, we repeated our 3D spheroid invasion assay following chemical inhibition of PIK3Cδ in fibroblast cells, using CAL-101 (idelalisib; a highly selective and potent PIK3Cδ inhibitor) (32). HMF or MRC5 cells were initially treated with different concentrations of CAL-101 for 24 hours, while the efficacy of CAL-101 inhibition on downstream targets of PIK3Cδ was validated (Supplemental Figure 7A). Moreover, treatment with CAL-101 had limited effect or no effect on fibroblasts' cell viability for the 24-hour period of treatment (Supplemental Figure 7B). Nevertheless, to avoid any misin-

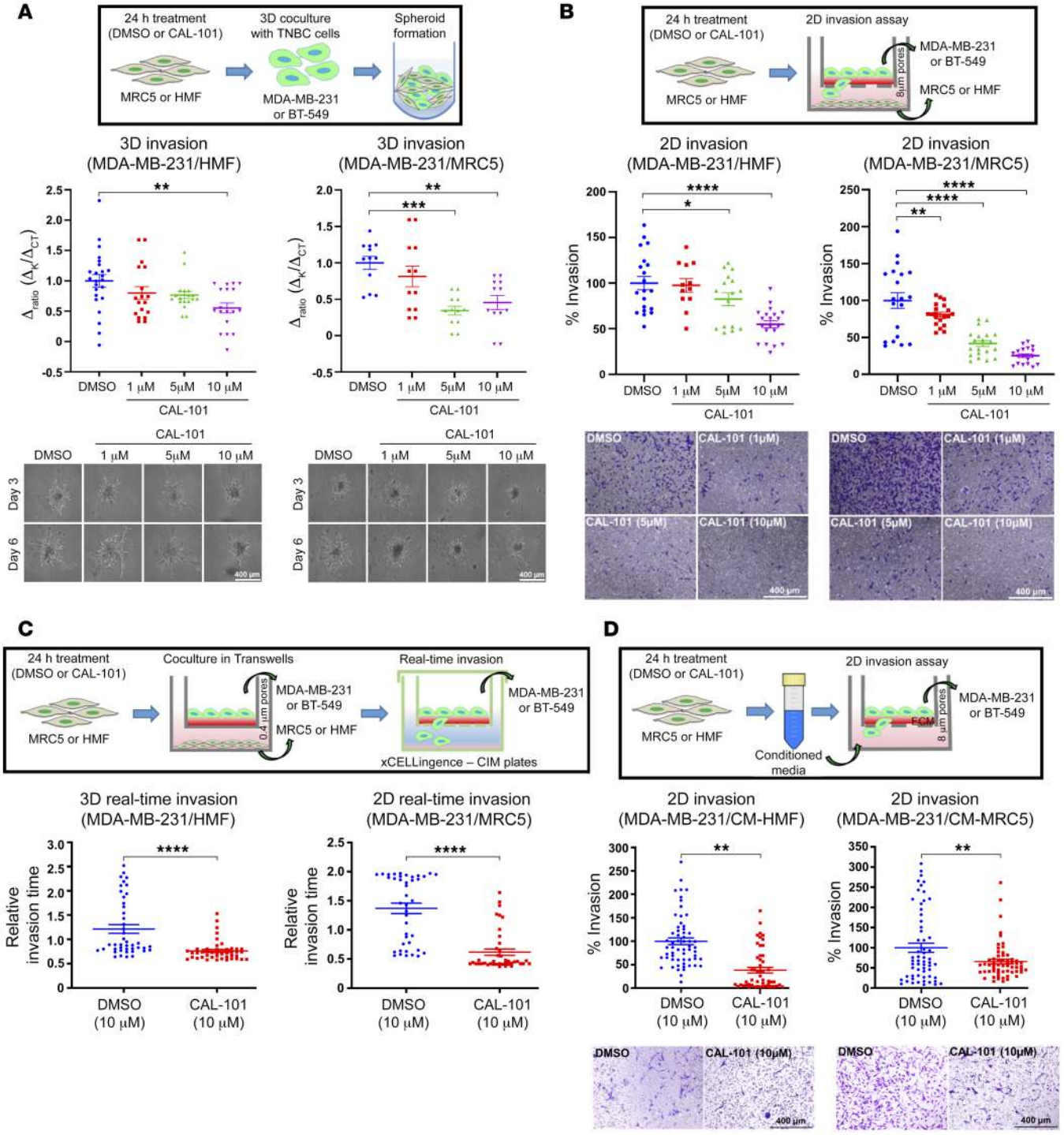

Figure 3. Effects of chemical inhibition of PIK3Cδ on TNBC 2D and 3D invasion. (**A**) 3D invasion assay: HMF (left panel) and MRC5 (right panel) cells were pretreated with DMSO or with 1, 5, or 10 μM CAL-101. After 24 hours, fibroblasts were cocultured with MDA-MB-231, and invasion was measured. Representative pictures are shown (n = 3 independent experiments, minimum 4 technical replicates). Significance was calculated using 1-way ANOVA and Tukey's multiple-comparisons tests. Results are expressed as mean ± SEM; $^{**}P < 0.01$, $^{***}P < 0.001$ vs. DMSO-treated fibroblasts. (**B**) 2D invasion assay: HMF (left) and MRC5 (right) cells were pretreated with DMSO or with 1, 5, or 10 μM CAL-101 for 24 hours and were seeded on the lower chamber of a Transwell. MDA-MB-231 cells were seeded on the Matrigel-coated upper chamber of the Transwell and cocultured with the fibroblasts. Twenty-four hours later, migrated MDA-MB-231 cells were fixed, stained, and counted (n = 3 independent experiments, minimum 3 technical replicates). Significance was calculated using 1-way ANOVA and Tukey's multiple-comparisons tests. Data are expressed as mean ± SEM; $^{*}P < 0.05$, $^{**}P < 0.01$, $^{****}P < 0.0001$ vs. DMSO-treated fibroblasts. (**C**) Real-time invasion assay: HMF (left) and MRC5 (right) cells were treated as in **B**. MDA-MB-231 cells were seeded on the upper chamber of the Transwell insert and were cocultured with the fibroblasts. After 24 hours, MDA-MB-231 cells were moved to CIM-Plates (xCELLigence, ACEA Biosciences) to monitor their relative invasion rate t. Significance was calculated using unpaired t test. Results are expressed as mean ± SEM; $^{****}P < 0.0001$. (**D**) Conditioned medium (CM) invasion assay: HMF (left) and MRC5 (right) cells were treated with vehicle or 10 μM CAL-101 in serum-free medium for 24 hours to obtain the CM. MDA-MB-231 cells were incubated with HMF or MRC5 CM for 2D invasion assays (n = 3 independent experiments, minimum 10 technical replicates). Significance was calculated using unpaired t test. Data are expressed as mean ± SEM; $^{**}P < 0.01$ vs. DMSO-treated fibroblasts' CM. Scale bars: 400 μm.

terpretations, fibroblasts were washed with PBS and counted with trypan blue, and only viable cells were used in cocultures with TNBC cells (MDA-MB-231 or BT-549) at a 1:1 ratio. CAL-101–pretreated fibroblasts showed a decrease in 3D spheroid invasion (Figure 3A and Supplemental Figure 8A), suggesting that the kinase activity of PIK3Cδ was, to a great extent, responsible for the observed results.

Intercellular communication sets the pace for transformed cells to survive and to thrive. Based on the initial setup of our assay (3D spheroid/cell coculture), we could not be certain whether the involvement of stromal PIK3Cδ in TNBC progression is a result of juxtacrine signaling (cell-to-cell contact–dependent) or a consequence of paracrine signaling due to secreted factors derived from fibroblasts that can alter the behavior of TNBC cells. Hence, we implemented a Transwell assay, in which HMF or MRC5 cells pretreated with CAL-101 were seeded on the lower chamber of the inserts and 24 hours later cocultured with TNBC cells plated on a Matrigel-coated top chamber to assess the 2D invasion potential of TNBC cells (Figure 3B and Supplemental Figure 8B). Using a similar experimental principle, we used the xCELLigence Real-Time Cell Analysis instrument (33) to monitor the real-time invasion rate of TNBC cells following coculturing with fibroblasts pretreated with CAL-101 (Figure 3C and Supplemental Figure 8C). Both assays revealed a reduction in invasiveness after inhibition of fibroblast PIK3Cδ activity. Similar results were observed when we implemented another method for indirect-contact cocultures using the CM of CAL-101–treated HMF or MRC5 cells and examining their effects on TNBC invasion (Figure 3D and Supplemental Figure 8D). Moreover, 2D invasion assays of either MDA-MB-231 or BT-549 cells cocultured with primary TNBC CAFs showed comparable results, further highlighting the role of fibroblast PIK3Cδ (Supplemental Figures 8E and 9).

To further demonstrate the contribution of PIK3Cδ to the observed phenotype and rule out any off-target effects, we repeated the 2D invasion assays by silencing PIK3Cδ and then performed a recovery experiment by reintroducing/overexpressing PIK3Cδ. As expected, by recovering PIK3Cδ levels (Supplemental Figure 10A), we reversed the decrease in invasion that was induced by genetic inhibition of PIK3Cδ (Supplemental Figure 10B).

Next, to examine the possibility of other fibroblast-expressed PI3K isoforms contributing to the decrease of TNBC cell invasion, in particular PI3KCγ, which can also be inhibited by CAL-101, we repeated the 2D invasion assays using various PI3K inhibitors (Supplemental Figure 11A). Treatment with AS252424 (a PIK3Cγ/α inhibitor) had minor effects on TNBC cell invasion, as compared with either CAL-101 or leniolisib (a PIK3Cδ inhibitor). Furthermore, use of the pan-PIK3C inhibitors PI-103 and NVP-BEZ235 had effects analogous to those of the PIK3Cδ inhibitors, further supporting the importance of PIK3Cδ in the observed phenotype (Supplemental Figure 11B). Finally, we verified that the observed effects on MDA-MB-231 cell invasion, following treatment with the different PIK3 inhibitors, were not based on a reduction of cell viability (Supplemental Figure 11C).

Taking together all combinations of cell lines and assays used, our results demonstrated that fibroblast PIK3Cδ promotes TNBC progression via paracrine regulatory mechanisms.

Integrated secretome/transcriptomic analyses reveal fibroblast PIK3Cδ–mediated paracrine mechanisms that promote TNBC progression. We and others (34, 35) have shown that coculture of stromal with BC cells leads to changes in protein expression supporting the hypothesis of crosstalk between different cell types. Changes of PIK3Cδ activity in fibroblasts can alter the intercellular communication between stromal and cancer cells, thereby affecting their biological properties. To gain insights into the paracrine mechanisms employed by fibroblasts to promote invasion in TNBC cells, we performed an integrated analysis of proteins secreted by HMF and MRC5 cells treated with CAL-101 and the transcriptome of MDA-MB-231 cells that were grown in a Transwell setup with CAL-101–treated MRC5 cells.

Based on our 2D/3D coculture results, we analyzed the PIK3Cδ-regulated secretome, using the Human L1000 Array (RayBiotech). HMF and MRC5 cells were treated with either DMSO or 10 μM CAL-101 for 24 hours, and cell culture supernatants were isolated and processed according to the manufacturer's instructions. By using differential expression analysis, we identified a total of 206 and 377 secreted proteins that were significantly regulated by CAL-101 treatment of HMF and MRC5 cells, respectively, at the $\log_2$ fold difference of |0.5| and a P value of ≤0.05. We found that 73 secreted proteins were common between CAL-101–treated HMF and MRC5 cells, providing evidence for a mechanism of fibroblast-mediated regulation of TNBC aggressiveness (Figure 4A and Supplemental Table 3). To gain additional insights into the similarities and differences in CAL-101–mediated effects on the secretome, we generated an upset plot of differentially expressed secreted proteins from CAL-101–treated HMF and MRC5 cells. As shown in Figure 4, B and C, CAL-101 upregulated a common set of 40 proteins and downregulated a set of 5 proteins in both HMF and MRC5 cells, while 28 proteins were differentially regulated by CAL-101 in HMF and MRC5.

With comprehensive profiling of CAL-101–mediated changes in the secretome of fibroblast cell lines established, next we investigated how these secreted proteins altered the transcriptional state of MDA-MB-231 cells. We cultured MDA-MB-231 cells in a Transwell along with CAL-101– or vehicle-treated MRC5 cells for 24 hours, and total RNA was extracted from MDA-MB-231 and processed as described before (36). Whole-transcriptome data showed a high degree of similarity between replicate samples and most significant variations between MDA-MB-231 cells cocultured with CAL-101–treated and untreated MRC5 cells (Supplemental Figure 12). The principal component analysis supports our hypothesis that inhibition of PIK3Cδ in fibroblasts has a paracrine effect on TNBC cells.

We next employed differential gene expression analysis using the DESeq2 pipeline (https://bioconductor.org/packages/release/bioc/html/DESeq2.html) to identify genes dysregulated in MDA-MB-231 cells as a consequence of inhibition of PIK3Cδ in MRC5 cells. We found 137 genes here at the false discovery rate Padj ≤ 0.05 (Figure 4D and Supplemental Table 4). Only 24 of 137 genes were significantly dysregulated at the false discovery rate Padj ≤ 0.05 and $\log_2$ fold difference of ≥|0.5| (Figure 4E). We validated the RNA-Seq analysis using an orthogonal approach of real-time qRT-PCR in independent experiments using a separate cohort including the effects of overexpression of PIK3Cδ on NR4A1 mRNA levels (Figure 4F and Supplemental Table 5). Among the most significantly modulated genes was NR4A1 transcription fac-

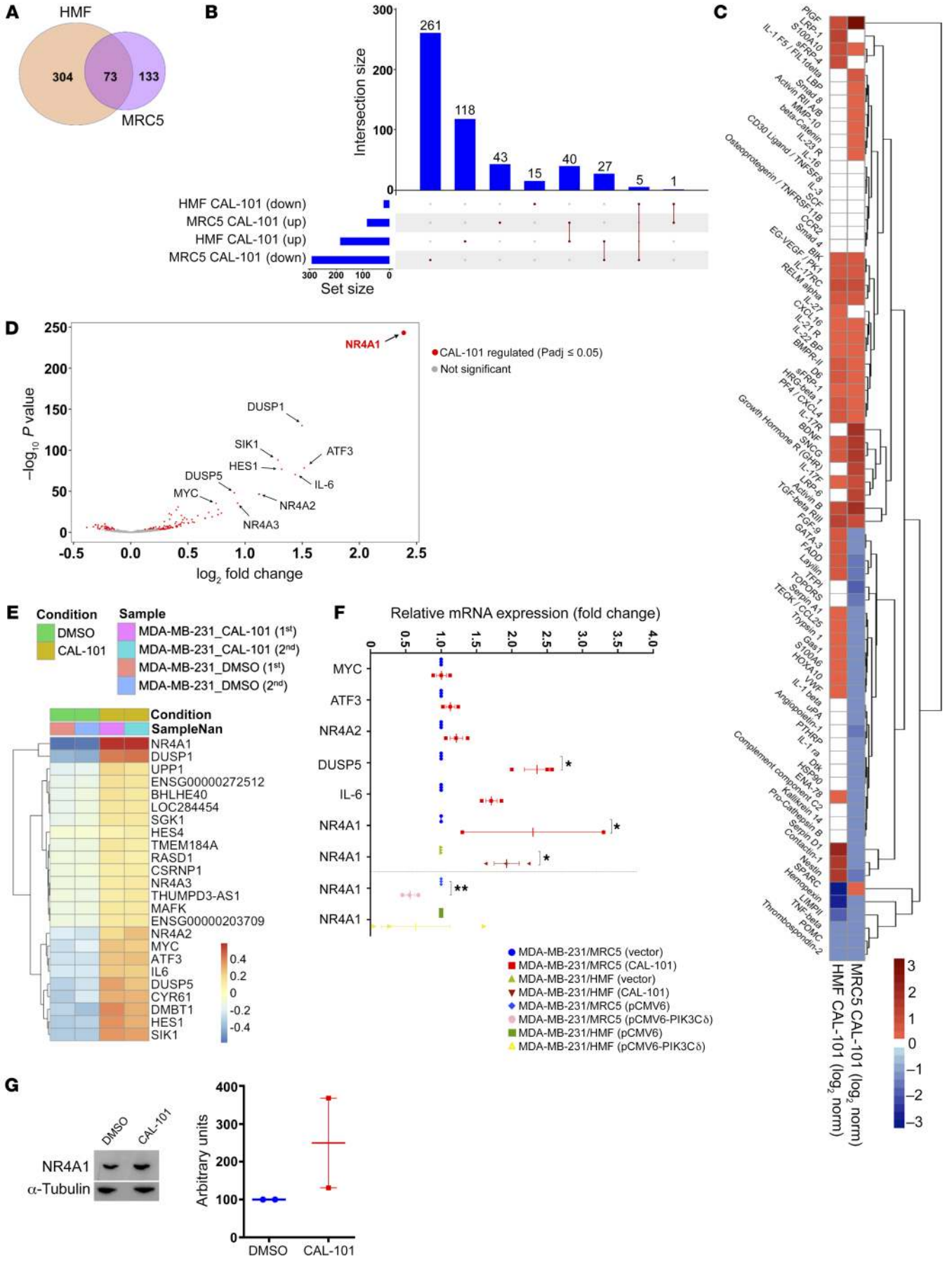
A
HMF
304
73
133
MRC5
B
Intersection size
261
118
43
15
40
27
5
1
HMF CAL-101 (down)
MRC5 CAL-101 (up)
HMF CAL-101 (up)
MRC5 CAL-101 (down)
Set size
C
MRC5 CAL-101 (log2 norm)
HMF CAL-101 (log2 norm)
D
−log10 P value
log2 fold change
NR4A1
DUSP1
SIK1
ATF3
HES1
DUSP5
IL-6
MYC
NR4A2
NR4A3
CAL-101 regulated (Padj ≤ 0.05)
Not significant
E
Condition
DMSO
CAL-101
Sample
MDA-MB-231_CAL-101 (1st)
MDA-MB-231_CAL-101 (2nd)
MDA-MB-231_DMSO (1st)
MDA-MB-231_DMSO (2nd)
F
Relative mRNA expression (fold change)
MYC
ATF3
NR4A2
DUSP5
IL-6
NR4A1
NR4A1
NR4A1
NR4A1
MDA-MB-231/MRC5 (vector)
MDA-MB-231/MRC5 (CAL-101)
MDA-MB-231/HMF (vector)
MDA-MB-231/HMF (CAL-101)
MDA-MB-231/MRC5 (pCMV6)
MDA-MB-231/MRC5 (pCMV6-PIK3Cδ)
MDA-MB-231/HMF (pCMV6)
MDA-MB-231/HMF (pCMV6-PIK3Cδ)
G
DMSO
CAL-101
NR4A1
α-Tubulin
Arbitrary units
DMSO
CAL-101

Figure 4. Global secretome analysis of CAL-101–treated fibroblasts and transcriptomics analysis of MDA-MB-231 cells. (**A**) To obtain CM from HMF and MRC5, cells were treated with vehicle or 10 μM CAL-101 in serum-free medium for 24 hours. CM was used to perform secretome analysis using the Human L1000 Array. Venn diagram showing differences in the secreted proteins significantly regulated by CAL-101 in HMF and MRC5 cells (Padj < 0.05 and $\log_2$ fold difference of ≥|0.5|). (**B**) UpSet plot showing common and unique CAL-101–regulated proteins significantly upregulated (up) or downregulated (down) in each data set (MRC5 and HMF). (**C**) Heatmap comparing $\log_2$ fold change of secreted proteins between CAL-101–treated HMF and MRC5 cells. (**D**) MRC5 cells were treated with either DMSO or 10 μM CAL-101 for 24 hours. Then cells were washed with PBS to remove the treatment, and complete fresh medium was added to each well. Five-micrometer inserts containing MDA-MB-231 cells were then added in the well containing previously treated MRC5. Twenty-four hours after coculture, cancer cells were collected for RNA extraction and subsequent RNA sequencing. Volcano plot showing the $\log_2$ fold change of genes in MDA-MB-231 cells that responded differently to CAL-101 treatment of MRC5 cells (DMSO:CAL-101). The $\log_{10}$ of *P* value, for significance in fold change, is plotted on the *y* axis. (**E**) Heatmap showing amounts by which the read counts of the top 24 regulated genes (ordered based on $\log_2$ fold change ≥|0.5| and Padj ≤0.05) deviate from the genes' average across all the samples. (**F**) qRT-PCR validation of genes identified via the RNA-seq and DESeq2 analysis. Significance was calculated using unpaired *t* tests. Results are expressed as mean ± SEM; $^*P < 0.05$, $^{**}P < 0.01$ vs. vector. (**G**) Western blotting of NR4A1 in MDA-MB-231 cells following coculture with CAL-101–treated MRC5 cells. α-Tubulin was used as loading control. Densitometry analysis of the blot is displayed as a ratio between CAL-101–treated and DMSO-treated cells.

tor, which was recently reported to be implicated in TNBC invasion (37). The increase of NR4A1 protein levels in MDA-MB-231 cells following coculture with CAL-101–treated MRC5 cells was also confirmed (Figure 4G).

Overall, these results show that pharmacological inhibition of PIK3Cδ in fibroblast cells not only alters its secretome, but also has a subtle paracrine effect on the gene expression of cancer cells.

Promotion of TNBC invasion via the fibroblast/epithelial-mediated PIK3Cδ–PLGF/BDNF–NR4A1 signaling pathway. Following confirmation of NR4A1 protein expression in different BC cell lines (Supplemental Figure 13A) and to further demonstrate its involvement in TNBC, we treated cells with cytosporone B, an agonist of NR4A1 (38), and examined its effects on the invasiveness of MDA-MB-231 and BT-549 cells. As expected, cytosporone B significantly decreased the invasiveness of TNBC cells (Figure 5A and Supplemental Figure 13B). On the contrary, silencing of NR4A1 increased the invasive ability of MDA-MB-231 cells (Figure 5B). Moreover, in the NR4A1-silenced cells, the effects of cytosporone B were almost completely abrogated (Supplemental Figure 13G). Silencing of NR4A1 was confirmed by qRT-PCR and Western blotting (Supplemental Figure 13, D and E), and in order to exclude possible off-target effects, NR4A2 and NR4A3 mRNA levels were analyzed by qRT-PCR in NR4A1-silenced cells (Supplemental Figure 13F).

Additionally, we investigated the effects of PIK3Cδ overexpression in MRC5 cells on the invasiveness of MDA-MB-231 cells pretreated with cytosporone B in order to increase their NR4A1 levels. As shown in Figure 5C, PIK3Cδ partly rescued the inhibitory effects of NR4A1 activation, demonstrating the PIK3Cδ-NR4A1 paracrine signaling axis between fibroblast and TNBC epithelial cells. To examine whether the effects of PIK3Cδ inhibition (CAL-101) on TNBC cell invasion are related to NR4A1 expression, we performed a 2D invasion assay in which MRC5 (or HMF) cells were treated with CAL-101 (or DMSO), while NR4A1 was silenced in MDA-MB-231 cells. As shown in Figure 5D and Supplemental Figure 13C, silencing of NR4A1 completely abrogated the effects of CAL-101 on TNBC cell invasion. Moreover, the NR4A1 silencing–mediated induction of invasion was abolished when fibroblasts were pretreated with CAL-101 (Figure 5D), which is due to the paracrine induction of NR4A1 expression caused by CAL-101 (Figure 5D) that balances the NR4A1 siRNA knockdown. Indeed, when NR4A1-silenced cancer cells were cocultured with CAL-101–treated fibroblasts, NR4A1 levels were restored (comparable to those of the control); thus, siNR4A1 MDA-MB-231 cells cocultured with CAL-101–treated MRC5 cells completely restore the baseline conditions in terms of NR4A1 levels as well as the invasion levels compared with those of MDA-MB-231 cocultured with MRC5 cells (Figure 5D, right). Together, these results suggest the existence of a direct association between fibroblast PIK3Cδ–mediated reduction of invasion and TNBC cells' NR4A1 levels.

Having built a comprehensive data set of secreted proteins from CAL-101–treated MRC5 cells and the transcriptome of MDA-MB-231 cocultured with CAL-101–treated MRC5 cells, we performed an integrated transcriptomics-proteomics analysis to unravel mechanisms used by stromal cells to promote invasion in malignant cells.

We hypothesized that secreted factors derived from CAL-101–treated MRC5 and HMF cells may alter cell-cell communication pathways and regulate the invasion of MDA-MB-231 cells by modulating the expression of invasion-related genes including *NR4A1*, which was shown to be overexpressed in our transcriptomic analysis (Supplemental Table 4). To test this hypothesis, we used the Ingenuity Pathway Analysis (IPA) software and literature mining to curate a list of potential PIK3Cδ-regulated secreted proteins that are enriched in cell migration/invasion pathways and are also known to modulate NR4A1 expression. Our analytical method, which is described in Supplemental Figure 14, identified several secreted factors ($n = 40$) that were directly involved in pathways regulating cellular movement or cell-to-cell signaling mechanisms (Supplemental Table 6), among which certain of them have been reported to have an association with *NR4A1* expression, including placental growth factor (PLGF) (39, 40) and brain-derived neurotrophic factor (BDNF) (ref. 41 and Supplemental Figure 15). Scatter plots displaying all secreted proteins from CAL-101–treated MRC5 and HMF cells while highlighting the list of potential candidates regulating NR4A1 expression in MDA-MB-231 cells are shown in Figure 6, A and B.

Previous studies have demonstrated that induction of NR4A1 by PLGF inhibits endothelial cell proliferation (42, 43), while PLGF can also impede tumor growth and metastasis (44). Moreover, BDNF has been described to have a role in BC progression (45), even though its exact role has not been completely clarified. Treatment of MDA-MB-231 or BT-549 cells with PLGF or BDNF confirmed its positive effects on NR4A1, supporting their contribution in the paracrine upregulation of NR4A1 mRNA/protein levels (Figure 6, C and D, and Supplemental Figure 16A). Moreover, PLGF and BDNF also led to a significant decrease in TNBC invasion (Figure 6E and Supplemental Figure 16B). Finally, we confirmed that silencing of either BDNF or PLGF in fibroblasts

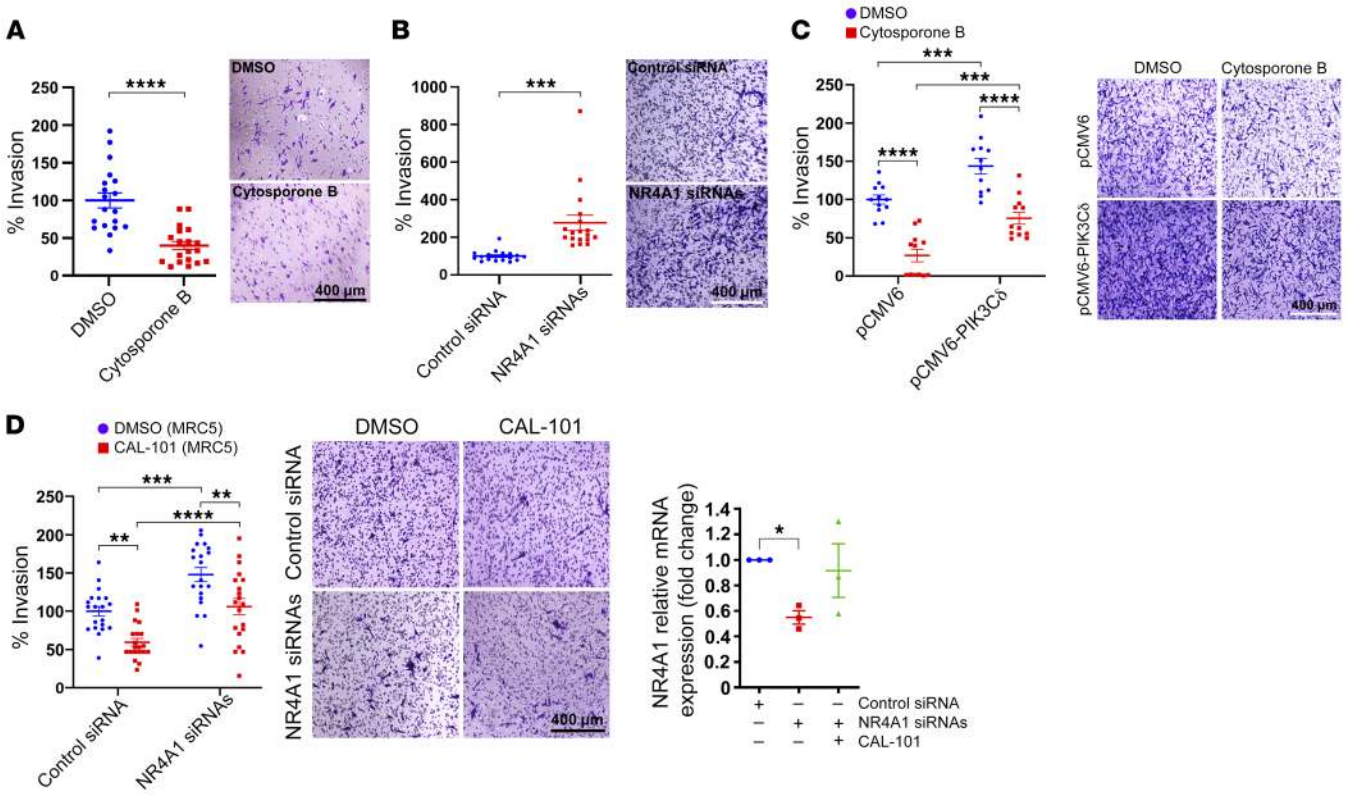

Figure 5. Effects of fibroblast PIK3Cδ expression on NR4A1-mediated invasion of TNBC cells. (**A**) 2D invasion assay: MDA-MB-231 cells were seeded on the Matrigel-coated upper chamber of the Transwell insert and were treated with DMSO or 5 μM cytosporone B. After 24 hours, migrated MDA-MB-231 cells were fixed, stained, and counted (n = 2 independent experiments, minimum 9 technical replicates). Significance was calculated using unpaired t test. Results are expressed as mean SEM; ****P < 0.0001 vs. DMSO-treated cells. (**B**) 2D invasion assay: MDA-MB-231 cells transfected with control or NR4A1 siRNAs were seeded as above. After 24 hours, migrated MDA-MB-231 cells were fixed, stained, and counted (n = 2 independent experiments, minimum 9 technical replicates). Significance was calculated using unpaired t test. Results are expressed as mean ± SEM; ***P < 0.001 vs. siRNA control–transfected cells. (**C**) Effects of PIK3Cδ overexpression in MRC5 on MDA-MB-231 invasion following pretreatment of MDA-MB-231 with 5 μM cytosporone B (n = 2 independent experiments, minimum 9 technical replicates). Significance was calculated using 2-way ANOVA and Tukey's multiple-comparisons tests. Results are expressed as mean ± SEM; ***P < 0.001, ****P < 0.0001 vs. the samples indicated in the graph. (**D**) Left and middle: MRC5 cells were treated with CAL-101 or DMSO. NR4A1 siRNA MDA-MB-231 or control siRNA cells were seeded on the Matrigel-coated upper chamber of a Transwell and cocultured with fibroblasts. After 24 hours, migrated MDA-MB-231 cells were fixed, stained, and counted (n = 3 independent experiments, minimum 6 technical replicates). Significance was calculated using 2-way ANOVA and Tukey's multiple-comparisons tests. Results are expressed as mean ± SEM; **P < 0.01, ***P < 0.001, ****P < 0.0001 vs. the samples indicated in the graph. Right: NR4A1 levels were evaluated in siRNA-transfected MDA-MB-231 cells before and after coculture with CAL-101–treated MRC5. Significance was calculated using 1-way ANOVA followed by Dunnett's tests. Results are expressed as mean ± SEM; *P < 0.05 vs. control. Scale bars: 400 μm.

attenuated the CAL-101–mediated reduction of TNBC cell invasion, further supporting the involvement of this pathway, while suggesting the existence of additional mechanisms implicated in the described phenotype (Supplemental Figure 17A). Interestingly, silencing of BDNF and/or PLGF did not affect TNBC invasion, suggesting that the PIK3Cδ effects are exerted during membrane trafficking and/or secretion of these factors and not at the gene/protein expression level. This is in accordance with previous reports describing a role of CAL-101 in downregulating secretion, rather than expression, of chemokines in stromal cocultures (32). In addition, silencing of BDNF and/or PLGF abolished the CAL-101 inhibitory effects on fibroblast-mediated invasion, without affecting basal invasion levels. This may be due to the experimental design, since silencing of a gene does not have an immediate effect on the respective total and/or secreted protein levels. Finally, it is worth mentioning that other mechanisms/factors could also contribute to the fibroblast-mediated invasion. Silencing of BDNF and PLGF was confirmed by qRT-PCR (Supplemental Figure 17B).

In summary, our results reveal a novel paracrine signal transduction pathway between fibroblasts and TNBC cells, encompassing PIK3Cδ–PLGF/BDNF–NR4A1 (Figure 6F), without ruling out the existence of other mechanisms contributing to the observed phenotype.

Pharmacological inhibition of fibroblast PIK3Cδ reduces BC tumor growth in vivo. Next, we used an orthotopic BC xenograft model where MDA-MB-231 or MDA-MB-231 with MRC5 cells were coinjected in the mammary fat pads of NOD/SCID mice in order to examine the effects of PIK3Cδ inhibition. After tumor formation and mouse randomization, perioral administration of CAL-101 or vehicle (30% PEG 400 plus 0.5% Tween-80) was initiated for both groups according to the scheme in Figure 7A.

As previously reported (46), cancer cells in the coinjected tumors (MDA-MB-231+MRC5) exhibited larger tumor volumes

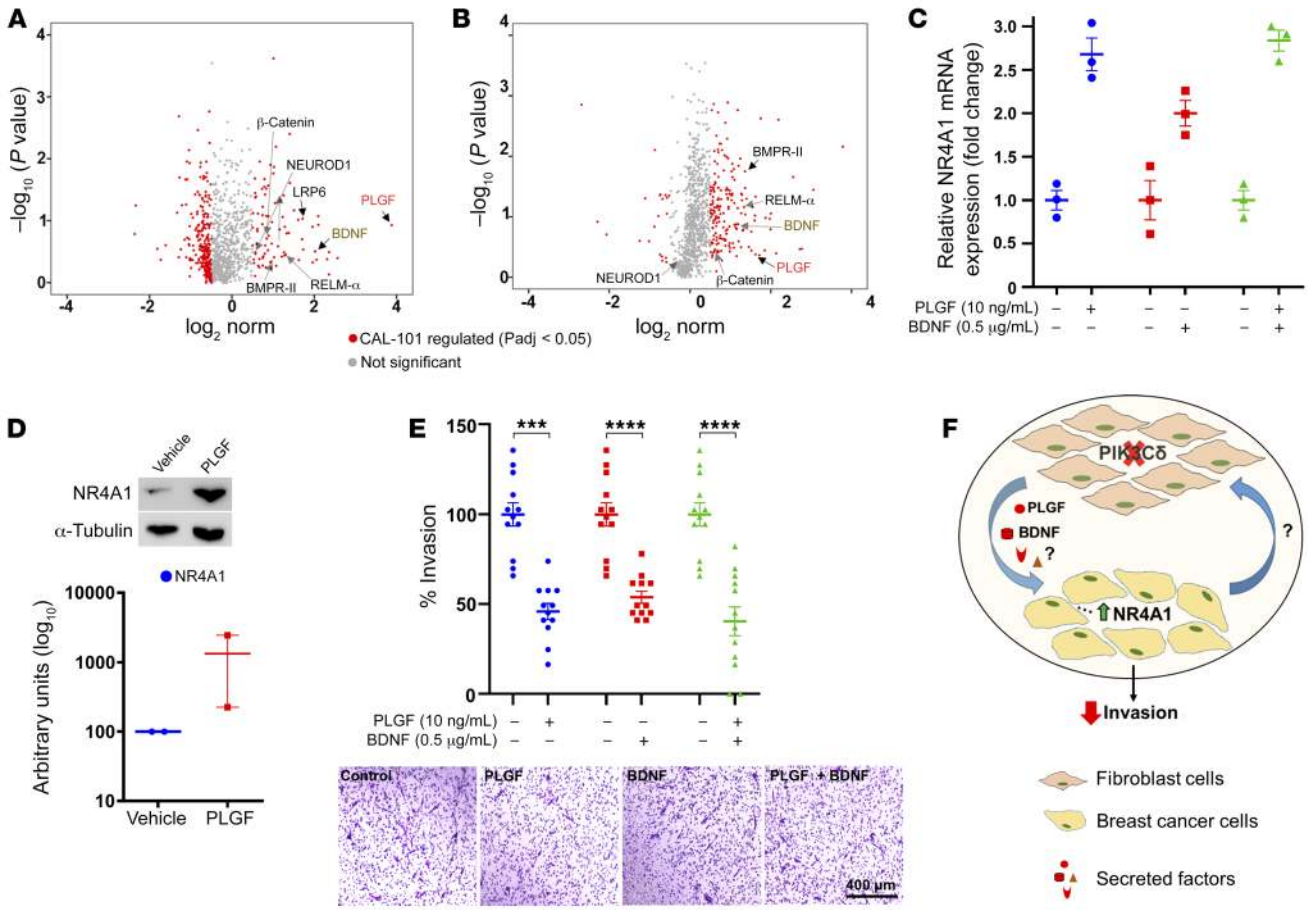

Figure 6. Effects of secreted factors including PLGF and BDNF on NR4A1-mediated invasion of TNBC cells. (**A**) Volcano plot showing the $\log_2$ fold change of secreted proteins in MRC5 cells that responded differentially to the CAL-101 treatment. The $\log_{10}$ of *P* value, for significance in fold change, is plotted on the *y* axis. (**B**) Volcano plot showing the $\log_2$ fold change of secreted proteins in HMF cells that responded differentially to the CAL-101 treatment. The $\log_{10}$ of *P* value, for significance in fold change, is plotted on the *y* axis. (**C**) qRT-PCR of NR4A1 expression levels in MDA-MB-231 cells following treatment with PLGF and BDNF. (**D**) Western blotting of NR4A1 in MDA-MB-231 cells following treatment with PLGF (10 ng/mL). GAPDH was used as loading control. Densitometry analysis of the blot is displayed as a ratio between PLGF-treated and vehicle-treated cells. (**E**) 2D invasion assay: MDA-MB-231 cells were seeded on the Matrigel-coated upper chamber of the Transwell insert and were treated with PLGF or BDNF or vehicle. After 24 hours, migrated MDA-MB-231 cells were fixed, stained, and counted ($n = 3$ independent experiments, minimum 4 technical replicates). Significance was calculated using unpaired *t* test. Results are expressed as mean ± SEM; $^{***}P < 0.001$, $^{****}P < 0.0001$ vs. vehicle-treated cells. (**F**) Schematic model depicting the paracrine signaling pathway between fibroblasts and TNBC cells. Inhibition of PIK3Cδ in fibroblasts leads to the secretion of different factors, including PLGF and BDNF, which promote the overexpression of *NR4A1* in epithelial cancer cells. NR4A1 acts as a tumor suppressor inhibiting the invasiveness of TNBC cells.

(Figure 7B) and a higher proliferative rate (Ki-67 labeling; Figure 7C). Moreover, CAL-101 treatment of MDA-MB-231 tumors did not significantly affect their in vivo growth (Figure 7B), in agreement with our cell-based data that demonstrated only a marginal inhibitory effect of CAL-101 on MDA-MB-231 proliferation (Supplemental Figure 18). Interestingly, MDA-MB-231+MRC5 tumors were reduced following treatment with CAL-101 (Figure 7B; day 14: 48.28% average reduction; day 21: 23.65% average reduction). The efficacy of CAL-101 on PIK3Cδ activity was validated by assessment of the expression of phosphorylated AKT (p-AKT) via IHC on tissue samples (Figure 7D). Moreover, the presence of human fibroblasts in MDA-MB-231+MRC5 tumors was confirmed in cryosection slides using a human anti-fibroblast antibody (Figure 7E). We also checked for $CD68^+$ cells (monocytes/macrophages); however, we detected only a small population of these tumor-infiltrating cells, which is consistent with the immunocompromised background of this mouse strain (Supplemental Figure 19). Finally, animals treated with CAL-101 did not display any significant changes in weight nor gross phenotypic changes, indicating that the treatment did not cause any adverse or toxic effects.

As a proof of concept of the potential use of PIK3Cδ inhibitors for BC treatment, we used the MMTV-PyMT transgenic model (47). MMTV-PyMT mice received daily oral administration of either control vehicle or CAL-101 (10 mg/kg) for a period of 6 weeks. Our results revealed a significant reduction in tumor growth following CAL-101 treatment (Figure 8, A and B, and Supplemental Figure 20, A and B). Moreover, the number of lung metastasis nodules was significantly reduced in the CAL-101 group compared with the control group, as evidenced by H&E staining and macroscopic observation of lung specimens (Figure 8C and Supplemental Figure 20, B and C). Furthermore, following CAL-101 treatment, the expression of p-AKT was decreased

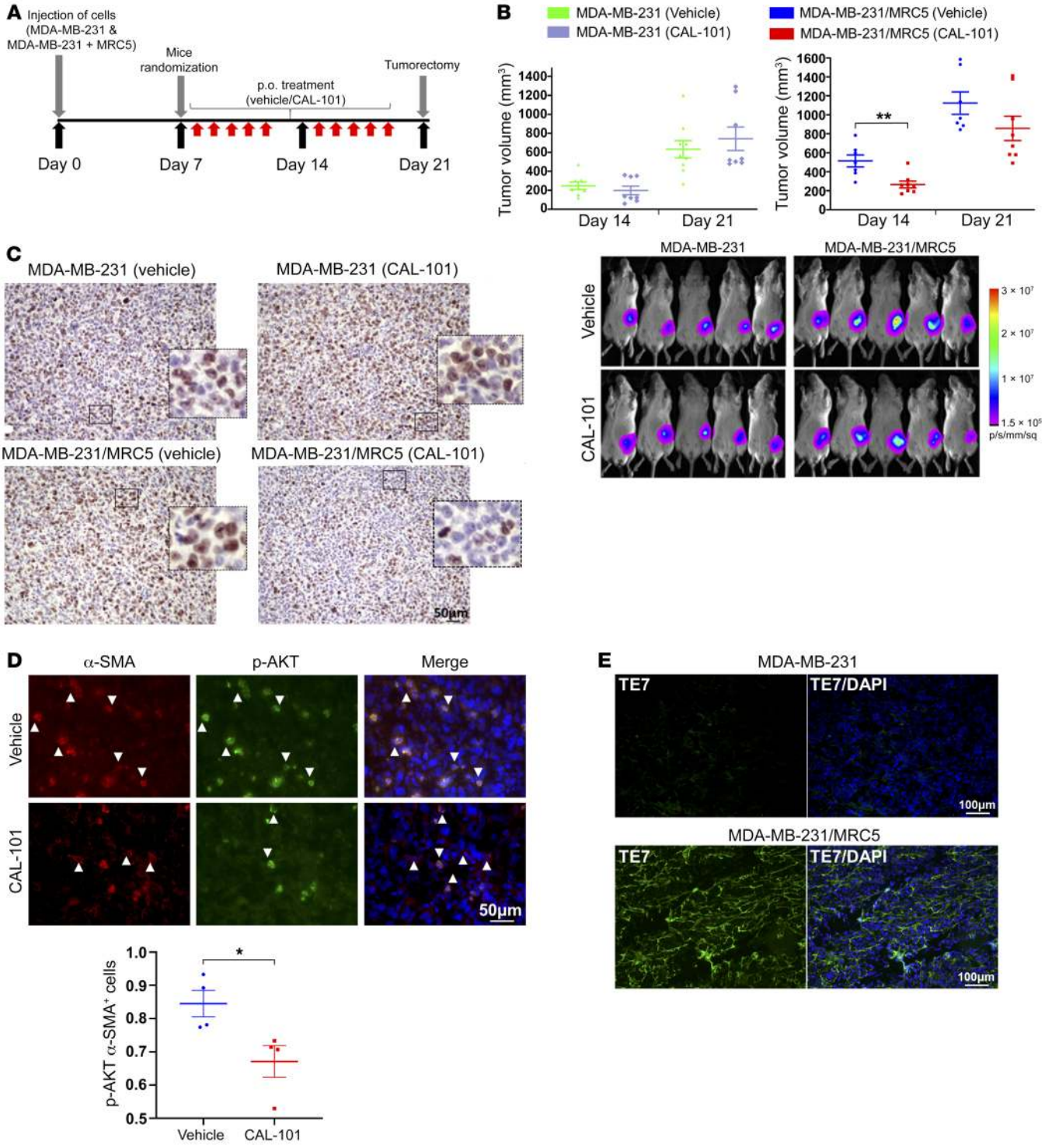

Figure 7. Effects of fibroblast PIK3Cδ inhibition on TNBC tumor growth in vivo. (**A**) Schematic representation of the in vivo experiment using NOD CB17 PRKDC/J mice. MDA-MB-231 (groups 1 and 2) and MDA-MB-231/MRC5 (groups 3 and 4) tumor cells were implanted s.c. on day 0. After randomization on day 7, treatment with CAL-101 was initiated in groups 2 and 4, whereas groups 1 and 3 were given vehicle. During the course of the study, the growth of the subcutaneously implanted primary tumors was determined twice weekly by luminescence and caliper measurement. (**B**) Top: Box-and-whisker plots comparing different groups at day 14 and day 21. Significance was calculated using unpaired *t* test. Results are expressed as mean SEM; $^{**}P < 0.01$. Bottom: Representative in vivo images of different groups, treated with vehicle or CAL-101. (**C**) Histological analysis of Ki-67 expression in representative tumor tissue sections of different groups. Original magnification, ×20. (**D**) Representative images of immunofluorescent staining of MDA-MB-231/MRC5 tumor cryosections for α-SMA and p-AKT^{Ser473} after DMSO or CAL-101 treatment. Significance was calculated using unpaired *t* test. Results are expressed as mean ± SEM; $^{*}P < 0.05$ vs. vehicle-treated tumors. Original magnification, ×40. (**E**) Representative images of immunofluorescence staining of tumor cryosections using TE-7 anti–human fibroblast antibody. Original magnification, ×20.

in tumor-infiltrating fibroblasts (α-SMA$^+$) (Figure 8D), as well as in macrophages (F4/80$^+$) (Figure 8E), while no changes were observed in the total PIK3Cδ levels of fibroblasts or macrophages (Supplemental Figure 20, D and E). In addition, as demonstrated in TNBC and fibroblast cell lines (Supplemental Figure 4C), PIK3Cδ was exclusively expressed in CAFs isolated from MMTV-PyMT tumors, while cancer cells had low/undetectable levels of PIK3Cδ, the expression of which did not change following coculturing with CM isolated from CAFs (Supplemental Figure 20F), further supporting the in vitro evidence that the effects of CAL-101 are cancer cell–independent. Finally, IHC analysis of MMTV tumors revealed an increased expression of NR4A1 along with PLGF and BDNF following CAL-101 treatment (Supplemental Figure 21), supporting our cell-based data.

Taken together, these results highlight the involvement of fibroblast-expressed PIK3Cδ in promoting BC growth in vivo.

High fibroblast PIK3Cδ expression correlates with poor patient outcome in TNBC. Finally, we investigated the plausible role of fibroblast (α-SMA$^+$) or tumor-expressed (cancer cells) PIK3Cδ in a clinical setting by analyzing a well-characterized TNBC patient cohort (n = 179) (48, 49). The clinicopathological parameters are summarized in Supplemental Table 7. PIK3Cδ expression was variable in both tumor (H score range 20–220) and surrounding cancer-associated fibroblasts (5%–100%), with high PIK3Cδ tumoral expression (H score >130 observed in 31 of 179 cases [17%]) whereas fibroblasts showed high PIK3Cδ (>85%) in 44 of 179 (25%) of the cases (Figure 9A and Supplemental Figure 22).

Analysis of the surrounding stromal (α-SMA$^+$) PIK3Cδ expression revealed PIK3Cδ as an independent prognostic factor for overall survival (OS) (P = 0.000285; Figure 9B) and disease-free survival (DFS) (P = 0.048; Figure 9C), indicative of fibroblast PIK-3Cδ's involvement in TNBC progression. Multivariate analyses demonstrated that PIK3Cδ in the surrounding cancer fibroblasts was also a prognostic factor for OS (P = 0.001) and DFS (P = 0.044) independent of age and nodal stage (Supplemental Table 8). Similar analyses revealed that high tumoral PIK3Cδ protein levels were associated with a significantly shorter OS (P = 0.0004) and DFS (P = 0.009) (Supplemental Figure 23, A and B), while tumoral PIK-3Cδ was a prognostic factor for OS (P = 0.006) and DFS (P = 0.028) independent of age, nodal stage, and lymphovascular invasion status (Supplemental Table 9). Interestingly, investigation of fibroblast PIK3Cδ in an ERα$^+$ patient cohort from Singapore (n = 73; P = 0.703) did not reveal any correlation with survival outcome (Figure 9D and Supplemental Tables 10–12).

We also used another approach to investigate the potential association of CAF-PIK3Cδ mRNA levels with survival outcomes of ERα$^+$, HER2$^+$, and TNBC subtypes, by deconvoluting bulk RNA-Seq samples from TCGA BC data using specific CAF and immune marker genes (Supplemental Table 13). As illustrated in Figure 9E, TNBC patients (n = 108) with high CAF-expressed PIK3Cδ levels had shorter OS compared with those with low CAF-expressed PIK3Cδ (P = 0.001), in agreement with our IHC data. Conversely, when we studied the bulk tumors, there was no significant association between PIK3Cδ mRNA levels and TNBC patients' survival outcome (P = 0.405; Supplemental Figure 23C), opposite to the IHC data, emphasizing the discrepancies that can arise in examining mRNA versus protein levels, which can lead to different conclusions. In addition, these results also highlight the importance of comprehensively analyzing the different cell types separately within the TME. Moreover, expression of CAF-PIK3Cδ mRNA levels was not predictive of survival for the ERα$^+$ BC subtype (n = 778, P = 0.0584; Figure 9F) — recapitulating the IHC data — nor for the HER2$^+$ subtype (n = 160, P = 0.684; Figure 9G), further underlining the significance of fibroblast-expressed PIK-3Cδ isoform in TNBC specifically.

We analyzed the association between the mRNA expression levels of CAF-PIK3Cα, β, and γ isoforms and patient survival for all BC subtypes. Our results revealed that in TNBC high CAF-expressed PIK3Cα (P = 0.01; Supplemental Figure 23D) or CAF-expressed PIK3Cβ (P = 0.01; Supplemental Figure 23E) was correlated with shorter OS, while there was no association of either PIK3Cα or PIK3Cβ with ERα$^+$ or HER2$^+$ BC patient survival (ERα$^+$ patients: PIK3Cα, P = 0.106; PIK3Cβ, P = 0.15; HER2$^+$ patients: PIK3Cα, P = 0.731; PIK3Cβ, P = 0.849). Regarding CAF-PIK3Cγ mRNA levels, there was no correlation with survival in either TNBC (Supplemental Figure 23F) or any of the other BC subtypes (ERα$^+$ patients: PIK3Cγ, P = 0.137; HER2$^+$ patients: PIK3Cγ, P = 0.943).

In conclusion, our results demonstrate the clinical significance of fibroblast-expressed PIK3Cδ in TNBC.

Discussion

TNBC represents an aggressive BC subtype where there remains an unmet clinical need; currently the recommended therapeutic approach in the neoadjuvant, adjuvant, and metastatic settings is based on chemotherapeutics (most often platinum-, anthracycline-, or taxane-based), with recent data suggesting roles for antibody-drug conjugates and immunotherapies (50–53). However, fewer than 30% of women with metastatic TNBC will survive 5 years after diagnosis (54). Sequencing and other "omics" have revealed an unexpected level of heterogeneity in TNBCs and led to identification of potential actionable targets (52).

However, translational research and clinical trials usually focus on targeting epithelial cancer cells. This is likely to diminish the contribution of reciprocal interactions between malignant and stromal cells that creates a local microenvironment, which fosters tumor growth and also influences responses to treatment (55). The prognostic and predictive significance of gene/protein expression signatures of the surrounding stroma has been well documented and could represent unexplored ground within the TME that could then be used to improve therapies and outcomes.

PKs are involved in every aspect of cell activity, and perturbation of their signaling can contribute to human diseases including malignancies (56–59). Pharmaceutical intervention targeting aberrant kinase signaling represents the major therapeutic approach, but although targeted therapies against PKs have improved the clinical outcome of patients, resistance to these treatments develops (60), emphasizing the need for the identification of new druggable targets.

Despite extensive research describing deregulated kinase activity in cancer cells, there has been no thorough and comprehensive investigation about how kinases expressed in stromal cells can influence tumor growth and malignant progression. Therefore, we focused on fibroblasts, the main stromal component in the TME, whose multiplex role in BC initiation, progres-

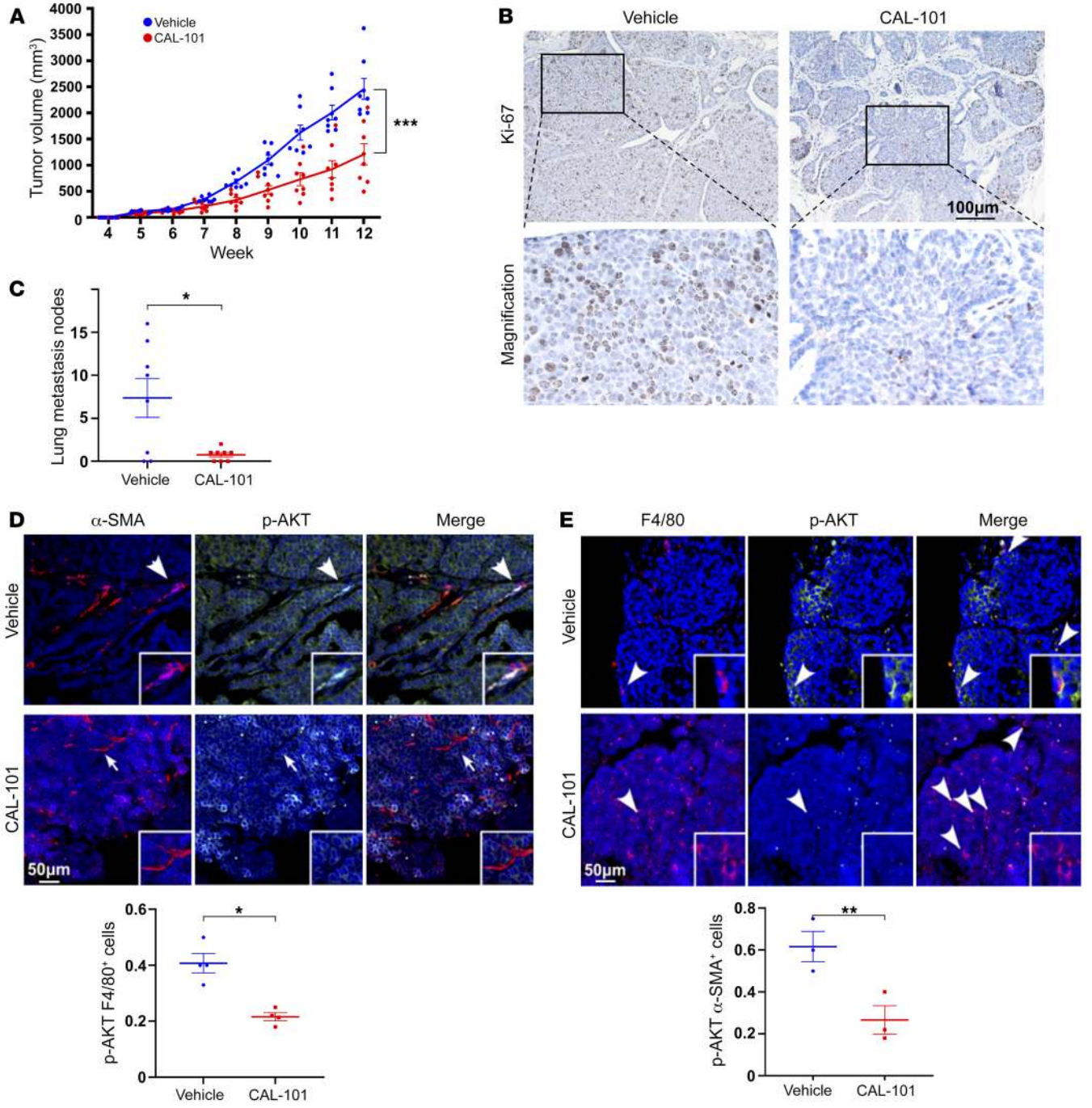

Figure 8. Effects of CAL-101 treatment on tumor growth of MMTV-PyMT transgenic mice. (**A**) Tumor volumes from MMTV-PyMT transgenic mice after vehicle or CAL-101 treatment (n = 8 mice per group). Individual values for each mouse are displayed. Significance was calculated using unpaired t test (week 12). Results are expressed as mean ± SEM; ***$P < 0.001$. (**B**) Representative images of IHC Ki-67 staining in the mammary tumor sections of MMTV-PyMT transgenic mice after vehicle or CAL-101 treatment. (**C**) Quantification of lung metastatic nodules in each group. Significance was calculated using unpaired t test. Results are expressed as mean ± SEM; *$P < 0.05$. Yellow and black dots represent mice that were sacrificed at week 12 or week 15 respectively. (**D**) Top: Representative images of immunofluorescent staining for α-SMA and p-AKT^{Thr308} in the mammary tumor sections of MMTV-PyMT transgenic mice after vehicle or CAL-101 treatment. Arrows indicate α-SMA$^+$ fibroblasts. Higher-magnification images are shown in the bottom right corners. Bottom: Quantification of p-AKT^{Thr308} immunofluorescent staining in tumor-infiltrating α-SMA$^+$ fibroblasts in the mammary tumors of MMTV-PyMT transgenic mice after vehicle or CAL-101 treatment. Significance was calculated using multiple t tests. Results are expressed as mean ± SEM; *$P < 0.05$ vs. vehicle-treated tumors. (**E**) Top: Representative images of immunofluorescent staining for F4/80 and pAKT^{Thr308} in the mammary tumor sections of MMTV-PyMT transgenic mice after vehicle or CAL-101 treatment. Arrows indicate F4/80$^+$ macrophages. Higher-magnification images are shown in the bottom right corners. Bottom: Quantification of pAKT^{Thr308} immunofluorescent staining in tumor-infiltrating F4/80$^+$ macrophages in the mammary tumors of MMTV-PyMT transgenic mice after vehicle or CAL-101 treatment. Significance was calculated using multiple t tests. Results are expressed as mean ± SEM; **$P < 0.01$ vs. vehicle-treated tumors.

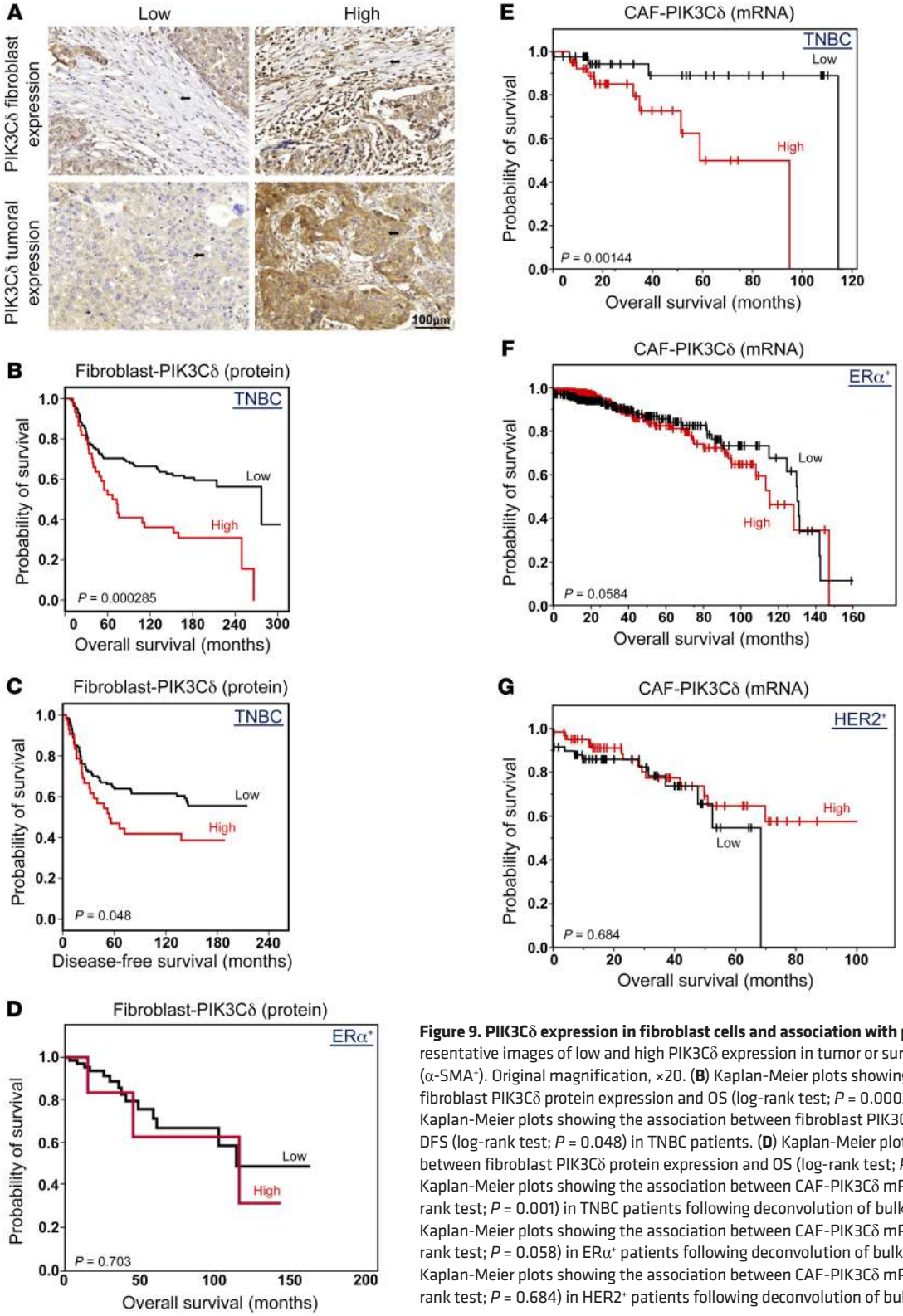

Figure 9. PIK3Cδ expression in fibroblast cells and association with patient survival. (**A**) Representative images of low and high PIK3Cδ expression in tumor or surrounding fibroblast cells (α-SMA$^+$). Original magnification, ×20. (**B**) Kaplan-Meier plots showing the association between fibroblast PIK3Cδ protein expression and OS (log-rank test; $P = 0.000285$) in TNBC patients. (**C**) Kaplan-Meier plots showing the association between fibroblast PIK3Cδ protein expression and DFS (log-rank test; $P = 0.048$) in TNBC patients. (**D**) Kaplan-Meier plots showing the association between fibroblast PIK3Cδ protein expression and OS (log-rank test; $P = 0.703$) in ERα$^+$ patients. (**E**) Kaplan-Meier plots showing the association between CAF-PIK3Cδ mRNA expression and OS (log-rank test; $P = 0.001$) in TNBC patients following deconvolution of bulk TCGA RNA-Seq samples. (**F**) Kaplan-Meier plots showing the association between CAF-PIK3Cδ mRNA expression and OS (log-rank test; $P = 0.058$) in ERα$^+$ patients following deconvolution of bulk TCGA RNA-Seq samples. (**G**) Kaplan-Meier plots showing the association between CAF-PIK3Cδ mRNA expression and OS (log-rank test; $P = 0.684$) in HER2$^+$ patients following deconvolution of bulk TCGA RNA-Seq samples.

sion, and therapy-resistance has been well described (7, 13, 14). We performed a kinome siRNA screening in 2 different fibroblast cell lines, aiming to identify kinases responsible for stroma-tumor crosstalk. Our siRNA screening/3D coculturing model was linked to an invasion readout assay that could be performed more easily and reliably with TNBC cell lines, considering their invasive potential, compared with the noninvasive and less aggressive ER$^+$ luminal BC cells. However, our findings do not rule out the possibility that these targets can also be linked to other BC subtypes. Ultimately this study aimed to identify targets associated with an

aggressive phenotype, invasion being the clearest readout. Nevertheless, the original screening is not designed to identify a mechanism of action, and therefore the target's effects could be diverse once studied further (e.g., in vivo).

Considering the limited available therapeutic options for TNBC, we focused on this subtype since the identification of new putative druggable targets for TNBC is fundamental. Among a subset of differently fibroblast-expressed kinases that could modulate TNBC progression, PIK3Cδ was one of the prominent hits. Despite the involvement of PI3K activity in tumor-stroma interactions (15), still the possibility of using PI3K inhibitors on fibroblasts has not been considered to date.

Given its almost exclusive expression in fibroblasts, PIK3Cδ could not have been identified by focusing solely on TNBC cells, further supporting that the contribution of the TME in cancer development and progression needs to be studied in detail. Using 2D and 3D coculturing models, we determined that fibroblast-expressed PIK3Cδ is integral in TNBC progression. We validated our findings using genomic approaches (loss- and gain-of-function experiments), and we assessed the effects of the chemical inhibition of PIK3Cδ, using a highly selective FDA-approved PIK3Cδ inhibitor (CAL-101/idelalisib) (61), confirming that the catalytic activity of fibroblast PIK3Cδ is required for its paracrine effects on TNBC cells. Mechanistically, using an integrated analysis of the fibroblast PIK3Cδ–regulated secretome and its paracrine-mediated transcriptomic changes in TNBC cells, we identified secreted factors and genes that represent key signaling pathways contributing toward the observed PIK3Cδ-induced tumor-promoting phenotype. We focused on the link between the overexpression of fibroblast-secreted factors, including PLGF and BDNF, and the upregulation of NR4A1 transcription factor in TNBC epithelial cells, after inhibition of fibroblast PIK3Cδ. NR4A nuclear receptors are involved in metabolic, cardiovascular, and neurological functions, as well as in inflammation and cancer (62–65). Despite the structural similarities of NR4A1, NR4A2, and NR4A3, they display distinctive roles and specific functions (66). Intriguingly, NR4A1 has been reported to act as a tumor suppressor implicated in TNBC proliferation, viability, migration, and invasion (37). Our results support a model in which inhibition of fibroblast-expressed PIK3Cδ impedes TNBC progression, by promoting the secretion of PLGF, BDNF, and other factors, which in turn lead to the paracrine upregulation of NR4A1 in TNBC cells (Figure 6F). The existence of additional direct and/or reciprocal signaling pathways originated from cancer cells toward fibroblasts, which could potentially affect PIK3Cδ expression and ultimately contribute to this phenotype, merits further investigation.

To examine the effects of fibroblast-expressed PIK3Cδ on TNBC growth in vivo, we initially attempted to generate stable PIK3Cδ-KO HMF and MRC5 cell lines and compare their involvement in tumor growth versus PIK3Cδ wild-type fibroblasts. However, PIK3Cδ-KO clones exhibited a relatively slow growth rate and, considering also the fact that fibroblasts can easily differentiate (67), led us to the alternative option of pharmacologically (CAL-101) inhibiting PIK3Cδ. CAL-101 had no effect when used as a treatment on MDA-MB-231 tumor growth, similarly to what we observed in our cell-based proliferation data when MDA-MB-231 cells were directly treated with CAL-101. Moreover, CAL-101 was administered orally in immune-deficient mice, which, combined with the lack of any MDA-MB-231 tumor inhibition, suggests that there were systemic responses initiated from other subpopulations of cells within the TME. This result, along with a recent report in which the authors showed that pharmacological inhibition of PIK3Cδ impedes in vivo tumor growth by targeting cancer cells and macrophages, further supports the stromal involvement of PIK3Cδ in BC and the potential use of PIK3Cδ inhibitors in a clinical setting.

In our immunocompromised xenograft model, we initially verified that the coinjection of fibroblasts (MDA-MB-231+MRC5) had an additive effect in tumor formation when compared with MDA-MB-231 cancer cells alone. More importantly, we observed a decrease in MDA-MB-231+MRC5 tumors following daily treatment with CAL-101. Considering that the only variable between the 2 mouse models was the introduction of fibroblasts, it is clear that the antitumor effects of CAL-101 were conferred via their actions on fibroblasts. Noteworthy, the tumor growth reduction that was observed on day 21 between MDA-MB-231+MRC5 CAL-101–treated tumors and MDA-MB-231+MRC5 vehicle-treated ones was borderline nonsignificant despite the 23.65% median reduction (it is worth mentioning that alternative statistical tests gave a significant *P* value). We attributed this to the progressive population dilution and decreased viability of human fibroblast cells (MRC5) as the tumor size increases, causing a reduction in relative potency of CAL-101 (as the dosage was left unchanged) on fibroblast PIK3Cδ and its paracrine consequences. Moreover, our results in MMTV-PyMT transgenic mice revealed a significant reduction in primary tumor growth and in metastasis following treatment with CAL-101. The downregulation of PIK3Cδ's activity in fibroblasts, apart from macrophages, implies a prospective additive, immune-independent mechanism of action of PIK3Cδ inhibitors for cancer treatment. In addition, as fibroblasts have been reported to influence a number of other immune cells, namely monocytes and macrophages (68, 69), the existence of additional PIK3Cδ-mediated paracrine signaling effects between different cell types could not be ruled out.

The translational significance of fibroblast-expressed PIK3Cδ was validated in a TNBC cohort, in which we revealed PIK3Cδ as a prognostic factor for outcomes (OS and DFS), providing strong evidence for the use of PIK3Cδ inhibitors in this setting in clinical trials. Interestingly, PIK3Cδ was also expressed in the cancer cell population of patients, possibly as a result of inflammatory processes, since it has been reported that PIK3Cδ can be activated by proinflammatory mediators (70). This can explain the low/undetectable protein levels of PIK3Cδ in our tested BC cell lines and in our animal models, considering the short period of the in vivo experiments. In light of new evidence of the existence of distinct TNBC subtypes (71, 72), an even more comprehensive profiling of TNBC patients can reveal a specific subgroup in which stromal/tumoral PIK3Cδ can epitomize a successful treatment strategy.

In conclusion, this study uncovers a tumor-promoting role of fibroblast-expressed PIK3Cδ in BC. Although our work predominantly focused on TNBC, fibroblasts represent the major cellular components within the TME in most cancers; therefore the involvement of PIK3Cδ in other BC subtypes and malignancies should be explored. Considering that local invasion and metastasis are the main causes of death in most types of cancer, this discovery

opens new potential therapeutic paths and supports the rationale for using PIK3Cδ inhibitors (as single or combined therapy) for the treatment of solid tumors, in which irregular activation of stromal PIK3Cδ occurs independently of the immunological landscape.

Methods

Study approval. This work obtained ethics approval by the North West–Greater Manchester Central Research Ethics Committee under the title Nottingham Health Science Biobank (NHSB), reference no. 15/NW/0685.

Sequencing data availability. RNA-Seq data were submitted to the NCBI BioProject Database (submission ID SUB7028041, BioProject ID PRJNA608606).

For all other materials and methods, please refer to Supplemental Methods.

Author contributions

TG and GG conceived the project and participated in the study design, planned and oversaw the execution of all the work, collated and analyzed most of the data, interpreted the results, and wrote most of the manuscript. AD, VV, KB, and GB performed most of the biochemical and cell-based experiments described herein. KS, TO, KK, L Li, and MD performed the RNA-Seq experiments and contributed to the interpretation of the results and writing of the respective parts of the manuscript. KS performed the secretome data analysis and the TCGA deconvolution analysis. SG, VN, and DLK performed the xenograft mouse model and the respective IHC analyses. L Lao, JC, PH, and ES performed all the experiments related to the MMTV-PyMT transgenic mouse model. PC, GBH, and FMGP performed the bioinformatic analysis related to the siRNA screening experiment. MA, EAR, and ARG performed the IHC staining and analyses on the TNBC patient cohort and analyzed the data. KY and SCL performed the IHC on the ER^+ patient cohort and analyzed the data. JS assisted with the interpretation of the clinical data and edited the manuscript. All authors read and approved the final manuscript.

Acknowledgments

We thank Margarita Andreadou for her help with the histology analysis and the Nottingham Health Science Biobank for the provision of tissue samples. A special thank you to Athanasios Giamas for helping with the preparation of the figures. We acknowledge the role of the Breast Cancer Now Tissue Bank in collecting and making available the samples used in the generation of this publication. We thank Michael Toss for his assistance with histopathology and Rosy Favicchio for the useful and stimulating discussions. We thank Enrico Frabetti for his endless patience and support. This work was supported by the Imperial Biomedical Research Centre and Experimental Cancer Medical Centre, Action Against Cancer, the Colin MacDavid Family Trust, the Joseph Ettedgui Charitable Foundation, Alessandro Dusi, and Julian and Cat O'Dell. Work at the Biomedical Sciences Research Center Alexander Fleming was supported by InfrafrontierGR/Phenotypos (MIS 5002135), which is funded by the Operational Programme Competitiveness, Entrepreneurship and Innovation (NSRF 2014–2020) and cofinanced by Greece and the European Union (European Regional Development Fund). This research was also partly supported by the Intramural Research Program of the NIH, National Institute of Environmental Health Sciences (ES101765).

Address correspondence to: Teresa Gagliano and Georgios Giamas, University of Sussex, School of Life Sciences, JMS Building, Falmer, Brighton BN1 9QG, United Kingdom. Phone: 44.0.127.387.3163; Email: t.gagliano@sussex.ac.uk (TG); g.giamas@sussex.ac.uk (GG).

KS's present address is: Bristol-Myers Squibb Co., Princeton, New Jersey, USA.

1. Bauer KR, Brown M, Cress RD, Parise CA, Caggiano V. Descriptive analysis of estrogen receptor (ER)-negative, progesterone receptor (PR)-negative, and HER2-negative invasive breast cancer, the so-called triple-negative phenotype: a population-based study from the California cancer Registry. *Cancer*. 2007;109(9):1721–1728.
2. Perou CM, et al. Molecular portraits of human breast tumours. *Nature*. 2000;406(6797):747–752.
3. Joyce JA, Pollard JW. Microenvironmental regulation of metastasis. *Nat Rev Cancer*. 2009;9(4):239–252.
4. Kalluri R, Zeisberg M. Fibroblasts in cancer. *Nat Rev Cancer*. 2006;6(5):392–401.
5. Quail DF, Joyce JA. Microenvironmental regulation of tumor progression and metastasis. *Nat Med*. 2013;19(11):1423–1437.
6. Bhowmick NA, Moses HL. Tumor-stroma interactions. *Curr Opin Genet Dev*. 2005;15(1):97–101.
7. Finak G, et al. Stromal gene expression predicts clinical outcome in breast cancer. *Nat Med*. 2008;14(5):518–527.
8. Costa A, et al. Fibroblast heterogeneity and immunosuppressive environment in human breast cancer. *Cancer Cell*. 2018;33(3):463–479.e10.
9. West RB, et al. Determination of stromal signatures in breast carcinoma. *PLoS Biol*. 2005;3(6):e187.
10. McAllister SS, Weinberg RA. Tumor-host interactions: a far-reaching relationship. *J Clin Oncol*. 2010;28(26):4022–4028.
11. Parsonage G, et al. A stromal address code defined by fibroblasts. *Trends Immunol*. 2005;26(3):150–156.
12. Tomasek JJ, Gabbiani G, Hinz B, Chaponnier C, Brown RA. Myofibroblasts and mechano-regulation of connective tissue remodelling. *Nat Rev Mol Cell Biol*. 2002;3(5):349–363.
13. Lu P, Weaver VM, Werb Z. The extracellular matrix: a dynamic niche in cancer progression. *J Cell Biol*. 2012;196(4):395–406.
14. McMillin DW, Negri JM, Mitsiades CS. The role of tumour-stromal interactions in modifying drug response: challenges and opportunities. *Nat Rev Drug Discov*. 2013;12(3):217–228.
15. Vanhaesebroeck B, Whitehead MA, Piñeiro R. Molecules in medicine mini-review: isoforms of PI3K in biology and disease. *J Mol Med*. 2016;94(1):5–11.
16. De Henau O, et al. Overcoming resistance to checkpoint blockade therapy by targeting PI3Kγ in myeloid cells. *Nature*. 2016;539(7629):443–447.
17. Koyasu S. The role of PI3K in immune cells. *Nat Immunol*. 2003;4(4):313–319.
18. Okkenhaug K, Graupera M, Vanhaesebroeck B. Targeting PI3K in cancer: impact on tumor cells, their protective stroma, angiogenesis, and immunotherapy. *Cancer Discov*. 2016;6(10):1090–1105.
19. Lucas CL, et al. Dominant-activating germline mutations in the gene encoding the PI(3)K catalytic subunit p110δ result in T cell senescence and human immunodeficiency. *Nat Immunol*. 2014;15(1):88–97.
20. Kang S, Denley A, Vanhaesebroeck B, Vogt PK. Oncogenic transformation induced by the p110β, -γ, and -δ isoforms of class I phosphoinositide 3-kinase. *Proc Natl Acad Sci U S A*. 2006;103(5):1289–1294.
21. Tzenaki N, Papakonstanti EA. p110δ PI3 kinase pathway: emerging roles in cancer. *Front Oncol*. 2013;3:40.
22. Conte E, et al. Inhibition of PI3K prevents the proliferation and differentiation of human lung fibroblasts into myofibroblasts: the role of class I P110 isoforms. *PLoS One*. 2011;6(10):e24663.

23. Puri KD, et al. Mechanisms and implications of phosphoinositide 3-kinase delta in promoting neutrophil trafficking into inflamed tissue. *Blood*. 2004;103(9):3448–3456.
24. Erdmann T, et al. Sensitivity to PI3K and AKT inhibitors is mediated by divergent molecular mechanisms in subtypes of DLBCL. *Blood*. 2017;130(3):310–322.
25. Karbownik MS, et al. Antipsychotic drugs differentially affect mRNA expression of genes encoding the neuregulin 1-downstream ErbB4-PI3K pathway. *Pharmacology*. 2016;98(1–2):4–12.
26. Vogel C, Marcotte EM. Insights into the regulation of protein abundance from proteomic and transcriptomic analyses. *Nat Rev Genet*. 2012;13(4):227–232.
27. Uhlén M, et al. Proteomics. Tissue-based map of the human proteome. *Science*. 2015;347(6220):1260419.
28. Lee JY, Hong SH, Shin M, Heo HR, Jang IH. Blockade of FLT4 suppresses metastasis of melanoma cells by impaired lymphatic vessels. *Biochem Biophys Res Commun*. 2016;478(2):733–738.
29. Owusu BY, et al. Targeting the tumor-promoting microenvironment in MET-amplified NSCLC cells with a novel inhibitor of pro-HGF activation. *Oncotarget*. 2017;8(38):63014–63025.
30. Togashi Y, et al. Homozygous deletion of the activin A receptor, type IB gene is associated with an aggressive cancer phenotype in pancreatic cancer. *Mol Cancer*. 2014;13:126.
31. Orzan F, et al. Genetic evolution of glioblastoma stem-like cells from primary to recurrent tumor. *Stem Cells*. 2017;35(11):2218–2228.
32. Hoellenriegel J, et al. The phosphoinositide 3′-kinase δ inhibitor, CAL-101, inhibits B-cell receptor signaling and chemokine networks in chronic lymphocytic leukemia. *Blood*. 2011;118(13):3603–3612.
33. Jacob J, et al. LMTK3 escapes tumour suppressor miRNAs via sequestration of DDX5. *Cancer Lett*. 2016;372(1):137–146.
34. Bochet L, et al. Adipocyte-derived fibroblasts promote tumor progression and contribute to the desmoplastic reaction in breast cancer. *Cancer Res*. 2013;73(18):5657–5668.
35. Soon PS, et al. Breast cancer-associated fibroblasts induce epithelial-to-mesenchymal transition in breast cancer cells. *Endocr Relat Cancer*. 2013;20(1):1–12.
36. Stebbing J, et al. LMTK3 confers chemoresistance in breast cancer. *Oncogene*. 2018;37(23):3113–3130.
37. Wu H, et al. Nuclear receptor NR4A1 is a tumor suppressor down-regulated in triple-negative breast cancer. *Oncotarget*. 2017;8(33):54364–54377.
38. Zhan Y, et al. Cytosporone B is an agonist for nuclear orphan receptor Nur77. *Nat Chem Biol*. 2008;4(9):548–556.
39. Zhao S, Zhou L, Niu G, Li Y, Zhao D, Zeng H. Differential regulation of orphan nuclear receptor TR3 transcript variants by novel vascular growth factor signaling pathways. *FASEB J*. 2014;28(10):4524–4533.
40. Zhou L, et al. Differential function and regulation of orphan nuclear receptor TR3 isoforms in endothelial cells. *Tumour Biol*. 2016;37(3):3307–3320.
41. Kuribara M, et al. Extracellular-signal regulated kinase regulates production of pro-opiomelanocortin in pituitary melanotroph cells. *J Neuroendocrinol*. 2011;23(3):261–268.
42. Liu D, Jia H, Holmes DI, Stannard A, Zachary I. Vascular endothelial growth factor-regulated gene expression in endothelial cells: KDR-mediated induction of Egr3 and the related nuclear receptors Nur77, Nurr1, and Nor1. *Arterioscler Thromb Vasc Biol*. 2003;23(11):2002–2007.
43. Su YT, et al. Monoubiquitination of filamin B regulates vascular endothelial growth factor-mediated trafficking of histone deacetylase 7. *Mol Cell Biol*. 2013;33(8):1546–1560.
44. Xu L, et al. Placenta growth factor overexpression inhibits tumor growth, angiogenesis, and metastasis by depleting vascular endothelial growth factor homodimers in orthotopic mouse models. *Cancer Res*. 2006;66(8):3971–3977.
45. Hondermarck H. Neurotrophins and their receptors in breast cancer. *Cytokine Growth Factor Rev*. 2012;23(6):357–365.
46. Rajaram M, Li J, Egeblad M, Powers RS. System-wide analysis reveals a complex network of tumor-fibroblast interactions involved in tumorigenicity. *PLoS Genet*. 2013;9(9):e1003789.
47. Guy CT, Cardiff RD, Muller WJ. Induction of mammary tumors by expression of polyomavirus middle T oncogene: a transgenic mouse model for metastatic disease. *Mol Cell Biol*. 1992;12(3):954–961.
48. Abd El-Rehim DM, et al. High-throughput protein expression analysis using tissue microarray technology of a large well-characterised series identifies biologically distinct classes of breast cancer confirming recent cDNA expression analyses. *Int J Cancer*. 2005;116(3):340–350.
49. Blamey RW, et al. Survival of invasive breast cancer according to the Nottingham Prognostic Index in cases diagnosed in 1990-1999. *Eur J Cancer*. 2007;43(10):1548–1555.
50. de Azambuja E, Ameye L, Paesmans M, Zielinski CC, Piccart-Gebhart M, Preusser M. The landscape of medical oncology in Europe by 2020. *Ann Oncol*. 2014;25(2):525–528.
51. Bardia A, et al. Sacituzumab govitecan-hziy in refractory metastatic triple-negative breast cancer. *N Engl J Med*. 2019;380(8):741–751.
52. Bianchini G, Balko JM, Mayer IA, Sanders ME, Gianni L. Triple-negative breast cancer: challenges and opportunities of a heterogeneous disease. *Nat Rev Clin Oncol*. 2016;13(11):674–690.
53. Nanda R, et al. Pembrolizumab in patients with advanced triple-negative breast cancer: phase Ib KEYNOTE-012 study. *J Clin Oncol*. 2016;34(21):2460–2467.
54. Henderson IC, et al. Improved outcomes from adding sequential Paclitaxel but not from escalating Doxorubicin dose in an adjuvant chemotherapy regimen for patients with node-positive primary breast cancer. *J Clin Oncol*. 2003;21(6):976–983.
55. Sounni NE, Noel A. Targeting the tumor microenvironment for cancer therapy. *Clin Chem*. 2013;59(1):85–93.
56. Blume-Jensen P, Hunter T. Oncogenic kinase signalling. *Nature*. 2001;411(6835):355–365.
57. Giamas G, et al. Kinases as targets in the treatment of solid tumors. *Cell Signal*. 2010;22(7):984–1002.
58. Krause DS, Van Etten RA. Tyrosine kinases as targets for cancer therapy. *N Engl J Med*. 2005;353(2):172–187.
59. Lemmon MA, Schlessinger J. Cell signaling by receptor tyrosine kinases. *Cell*. 2010;141(7):1117–1134.
60. Stebbing J, et al. Characterization of the tyrosine kinase-regulated proteome in breast cancer by combined use of RNA interference (RNAi) and stable isotope labeling with amino acids in cell culture (SILAC) quantitative proteomics. *Mol Cell Proteomics*. 2015;14(9):2479–2492.
61. Somoza JR, et al. Structural, biochemical, and biophysical characterization of idelalisib binding to phosphoinositide 3-kinase δ. *J Biol Chem*. 2015;290(13):8439–8446.
62. Boudreaux SP, et al. Drug targeting of NR4A nuclear receptors for treatment of acute myeloid leukemia. *Leukemia*. 2019;33(1):52–63.
63. Close AF, Dadheech N, Villela BS, Rouillard C, Buteau J. The orphan nuclear receptor Nor1/Nr4a3 is a negative regulator of β-cell mass. *J Biol Chem*. 2019;294(13):4889–4897.
64. Medunjanin S, et al. DNA-dependent protein kinase (DNA-PK) permits vascular smooth muscle cell proliferation through phosphorylation of the orphan nuclear receptor NOR1. *Cardiovasc Res*. 2015;106(3):488–497.
65. Munnur D, et al. NR4A nuclear receptors target poly-ADP-ribosylated DNA-PKcs protein to promote DNA repair. *Cell Rep*. 2019;26(8):2028–2036.e6.
66. Safe S, Jin UH, Morpurgo B, Abudayyeh A, Singh M, Tjalkens RB. Nuclear receptor 4A (NR4A) family — orphans no more. *J Steroid Biochem Mol Biol*. 2016;157:48–60.
67. Kalluri R. The biology and function of fibroblasts in cancer. *Nat Rev Cancer*. 2016;16(9):582–598.
68. Chomarat P, Banchereau J, Davoust J, Palucka AK. IL-6 switches the differentiation of monocytes from dendritic cells to macrophages. *Nat Immunol*. 2000;1(6):510–514.
69. Erez N, Truitt M, Olson P, Arron ST, Hanahan D. Cancer-associated fibroblasts are activated in incipient neoplasia to orchestrate tumor-promoting inflammation in an NF-κB-dependent manner. *Cancer Cell*. 2010;17(2):135–147.
70. Whitehead MA, Bombardieri M, Pitzalis C, Vanhaesebroeck B. Isoform-selective induction of human p110δ PI3K expression by TNFα: identification of a new and inducible PIK3CD promoter. *Biochem J*. 2012;443(3):857–867.
71. Jiang YZ, et al. Genomic and transcriptomic landscape of triple-negative breast cancers: subtypes and treatment strategies. *Cancer Cell*. 2019;35(3):428–440.e5.
72. Rueda OM, et al. Dynamics of breast-cancer relapse reveal late-recurring ER-positive genomic subgroups. *Nature*. 2019;567(7748):399–404.